REPUBLIC OF TURKEY

ALTINBAŞ UNIVERSITY

Institute of Graduate Studies

Civil Engineering

FINITE ELEMENT ANALYSIS OF REPAIR OF CONTINUOUS REINFORCED CONCRETE BEAMS WITH NEAR SURFACE MOUNTED REINFORCEMENT

Fatimaalzhra SHAMMARI

Master's Thesis

Supervisor

Prof.Dr. Zeki HASGUR

Istanbul,2022

FINITE ELEMENT ANALYSIS OF REPAIR OF CONTINUOUS REINFORCED CONCRETE BEAMS WITH NEAR SURFACE MOUNTED REINFORCEMENT

Fatimaalzhra SHAMMARI

Civil Engineering

Master's Thesis

ALTINBAŞ UNIVERSITY

2022

The thesis titled "FINITE ELEMENT ANALYSIS OF REPAIR OF CONTINUOUS REINFORCED CONCRETE BEAMS WITH NEAR SURFACE MOUNTED REINFORCEMENT" prepared by FATIMAALZHRA SHAMMARI and submitted on 23/02/ 2022 has been **accepted by majority of votes** for the degree of Master of Science in Civil Engineering.

Prof. Dr.Zeki HASGUR

Supervisor

Thesis Defense Jury Members:

Prof.Dr. Zeki HASGUR	Faculty of Engineering and Architecture Altinbas Universie	_____
Prof. Dr. Tuncer CELIK	Faculty of Engineering and Architecture, Altinbas University	_____
Asst. Prof. Dr. Erdem DAMCI	Faculty of Engineering Istanbul University-Cerrahpasa	_____

I hereby declare that this thesis/dissertation meets all format and submission requirements of a …… (Master's/PhD) thesis/dissertation.

Submission date of the thesis to the Graduate Education Institute: ___/___/___

I hereby declare that all information/data presented in this graduation project has been obtained in full accordance with academic rules and ethical conduct. I also declare all unoriginal materials and conclusions have been cited in the text and all references mentioned in the Reference List have been cited in the text, and vice versa as required by the abovementioned rules and conduct

Fatimaalzhra SHAMMARI

Signature

ABSTRACT

FINITE ELEMENT ANALYSIS OF REPAIR OF CONTINUOUS REINFORCED CONCRETE BEAMS WITH NEAR SURFACE MOUNTED REINFORCEMENT

Shammari, Fatimaalzhra,

M.Sc., Civil Engineering, Altınbaş University,

Supervisor: Prof. Dr. Zeki HASGUR

Date: February /2022

Pages: 58.

In the current thesis, different methods of repairing a pre-cracked reinforced concrete beam (rcb) were reviewed and described briefly. Afterwards, Near surface mounted (NSM) technique was used to simulate reinforcement of a pre-cracked RCB using carbon fiber reinforced polymer (CFRP) laminated layer. to do this end, Firstly, Based on previous experimental and analytical studies the limitations of the dimensions were specified and then using MINITAB software, Taguchi L9 orthogonal array design of experiment (Doe) applied to optimize the number of simulations and find the best dimensions for the reinforcement. subsequently, Abaqus software used to analyze the flexural behavior of the NSM-CFRP pre-cracked RCB. Finally, Force-Deflection curves were exported from the simulation results and the best reinforcing pattern was selected.

Keywords: Finite Element Modeling, Optimization, Reinforced Concrete Beams, Fiber Reinforced Polymers, Abaqus

TABLE OF CONTENTS

Pages

LIST OF TABLES

Pages

LIST OF FIGURES

Pages

LIST OF ABBREVIATIONS

ASTM : American Society for Testing and Materials

ACI : American Concrete Institute

FRP : Fiber Reinforced Polymer

RCB : Reinforced Concrete Beam

CFRP : Carbon Fiber Reinforced Polymer

BFRP : Basalt Fiber Reinforced Polymer

GFRP : Glass Fiber Reinforced Polymer

LIST OF SYMBOLS

f_y : Yield stress

E : Modulus of elasticity

A_s : Area of bar reinforcement at tension zone

$\acute{A}s$: Area of bar reinforcement at compression zone

a : Depth of equivalent rectangular compressive stress block

$\acute{f}s$: Cylinder compressive strength of concrete

ε_u : Ultimate concrete strain

ε : Strain in concrete

1. INTRODUCTION

1.1 REINFORCED CONCRETE BEAMS

Concrete is one of the main materials of all constructions due to the high strength, specifically compressive strength. However, low tensile strength of the concrete is the weakness of this artificial composite. Therefore, strengthening is needed for concrete for the applications which require high tensile strength such as structural parts in constructions and bridges like beams and columns. Commonly, the reinforcement is in the shape of reinforcing bars and welded wire made by steel embedded inside of the concrete. Steel reinforced concrete beams are the most common version of reinforced beams which have a decent tensile strength as well as appropriate compressive strength. Despite the high tensile strength of the embedded steel inside the concrete beam, still cracking occurs in the bottom part of the beams and with increasing the load they propagate and with progressing the crack propagations the beam failure happens. Furthermore, based on the ACI code, different forms of reinforcements such as structural steel, steel pipe, steel tubing, and high-strength steel tendons can be utilized to reinforce the concrete in terms of increasing tensile strength [1]. Several other methods have been also investigated in order to find the most economical reinforcing method of the concrete to reach to the same tensile strength for the reinforced concrete. One of these methods is using short fibers of different materials such as steel, fiberglass, etc. The main and critical physical properties of reinforcing steel for reinforced concrete design calculations are yield stress (f_y) and elastic modulus (E).

The tensile yield stress of steel is measured by different tests such as tensile test based on ASTM standards. Usually, the physical properties of the steel used in the concrete such as yield ductility and elastic modulus are given and based on these parameters the final physical properties of reinforced concrete beam or other structures can be calculated. The elastic modulus of carbon reinforcing steel which is the curve slope of the elastic region in the stress–strain curve, differs over a very small range and has been accepted as about 200 GPa. The general stress-strain curve of the steel can be seen in Fig. 1.1. Furthermore, the idealized stress-strain diagram of the steel is shown in Fig. 1.2 to estimate the main properties of the material and separate the elastic and plastic region in the graph.

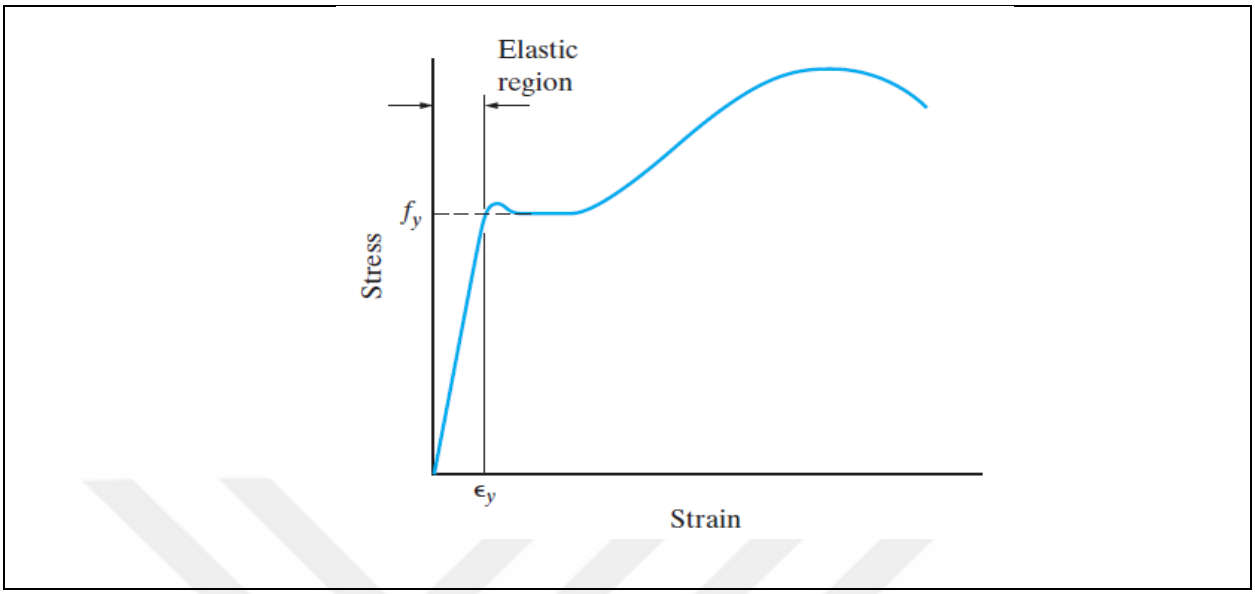

Figure 1.1: Schematic of stress–strain curve of the reinforcing steel measured by tensile test [2]

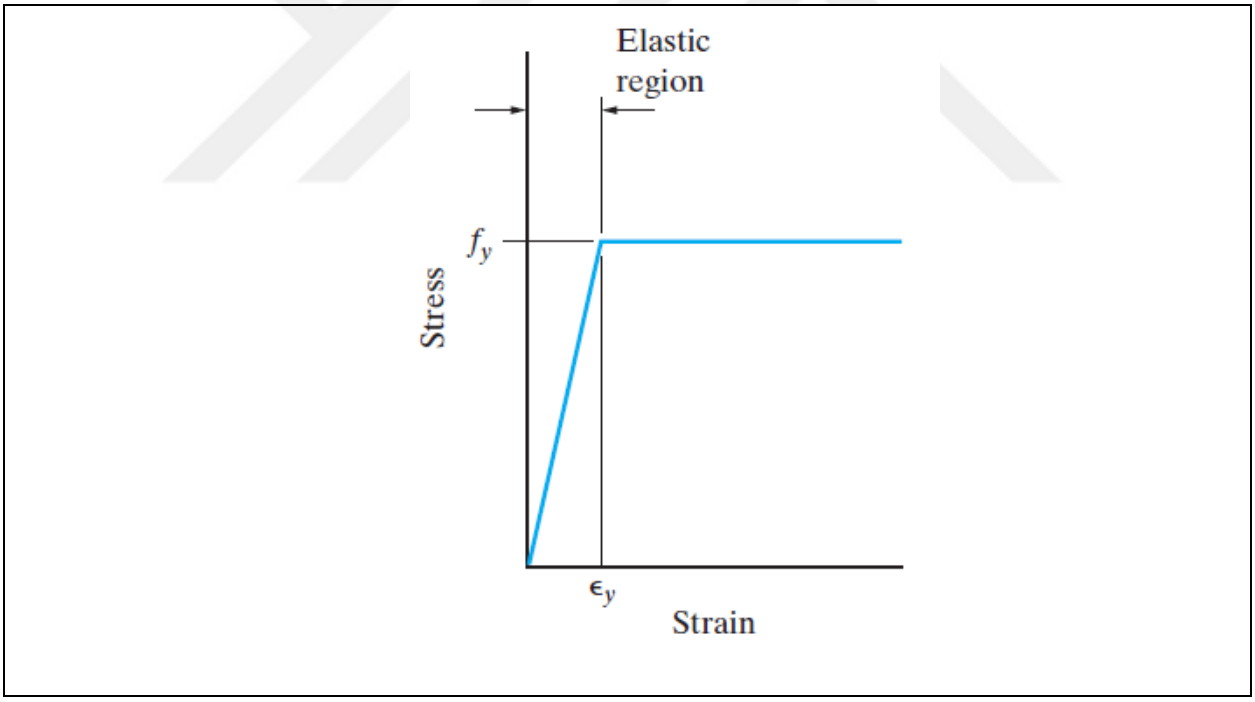

Figure 1.1: Stress–strain diagram for reinforcing steel (idealized curve) [2]

1.2 DIFFERENT TYPES OF REINFORCED CONCRETE BEAMS

One of the main parts of the structures and constructions is the reinforced concrete beams that can backing the flexural and transverse weight and force which generally rest on supports. The most common classification of the Beams can be identified as simple, continuous, semi-continuous, cantilever, and T-beams.

1.2.1 Simple Concrete Beams

One of the main and usually used types of the beams is simple concrete beam. Simple concrete beams are beams having supports with a single span at the end, and without any restraint at region of the support. Simple beam is also well known as simply supported beam. Restraint means a rigid connection or anchorage at the support.

1.2.2 Continuous Beam

A continuous beam is one that rests on more than two supports. It can be a single continuous beam for the full length of the structure with intermediate column or wall supports, or a single continuous beam for the entire length of the structure with intermediate column or wall supports.

1.2.3 Semi-Continuous Beam

A beam having two spans with or without constraint at the two extreme ends is referred to as a semi-continuous beam.

1.2.4 Cantilever Beam

Cantilever beams are supported on one end and extend beyond the support or wall on the other.

1.3 FIBER REINFORCED CONCRETES

The integrity of the structures can be enhanced and modified by adding fibrous materials to the concrete and make fiber reinforced concrete (FRC). These composites include different types of long and short discrete fibers with different shapes which are homogeneously dispersed and arbitrarily oriented. These materials can be made by steel fibers, glass fibers, synthetic fibers and

natural fibers, which each of them can change the mechanical and structural properties of reinforced concrete beam, significantly.

The listed advantages of employing FRPs are as follows:

a) Advance concrete strength without increasing the price of it.

b) Increases tensile strengthening in various directions (This characteristic is the difference between using FRPs and rebar, because in using rebar, the strengthening direction is limited to just one direction while we have strengthening in all direction with adding FRPs to the reinforced concrete beams).

c) Enhance resistance to freeze-thaw

d) Enhance explosive spalling in case of a severe fire

e) Improve impact– and abrasion–resistance

f) Improve the plastic shrinkage resistance after curing

g) Diminish steel reinforcement necessities

h) Enhance ductility

1.4 VARIOUS REPAITING TECHNIQUES FOR CONCRETE CRACK

Many techniques and methods have been used to repair the occurred cracks and prevent the crack growth on the structures such as beams and columns. These methods are epoxy injection, routing and sealing, grouting, stitching, drilling and plugging, gravity filling of cracks in concrete. In this section, the specifications and details related to each of these methods are mentioned. Moreover, the selection criteria for different method and various types of cracks have will be discussed below.

Appropriate technique of crack repairing for the reinforced concrete beams must be chosen with considering the initial cause and propagation rate and direction of the cracks on the beam. As soon as detecting the reason and classification of the cracks, the best repair method can be chosen and implemented. For instance, if the reason of crack initiation and propagation was because of drying shrinkage, then it means it will be stabilized and stopped after a while. Also, in another case, if the

reason of crack initiation cracks is because of a continuing foundation settlement, restoration cannot solve the problem until settlement problem is resolved.

1.4.1 Epoxy injection

In the case that the length of the crack is lower than 0.05mm, epoxy injection technique can be very useful and common method. The entrance and venting ports are usually initiated at close intervals via the cracks, the fracture is sealed on exposed surfaces, and the epoxy is injected under pressure. Epoxy injection has been used to repair fractures in buildings, bridges, dams, and other concrete structures with great effectiveness (ACI 503R). However, unless the cracking's source is addressed, it will most likely repeat around the initial fracture.

1.4.2 Routing and Sealing of Cracks

In circumstances when remedial repair is required but structural repair is not, crack routing and sealing may be used. This method entails growing the crack's size across its exposed face, then filling and sealing it with a good joint sealant (Fig. 1.3). The method works well on horizontal surfaces that are roughly flat, such as floors and pavements. Routing and sealing, on the other hand, may be done on both vertical and curved surfaces (with a non-sag sealant) (pipes, piles and pole). It's possible to utilize a concrete saw, hand tools, or pneumatic equipment. After that, the groove is cleaned using air, sand, or water blasting and dried. A bond breaker may be used at the bottom of the groove to allow the sealant to change form without putting too much stress on it (Fig. 1.4).

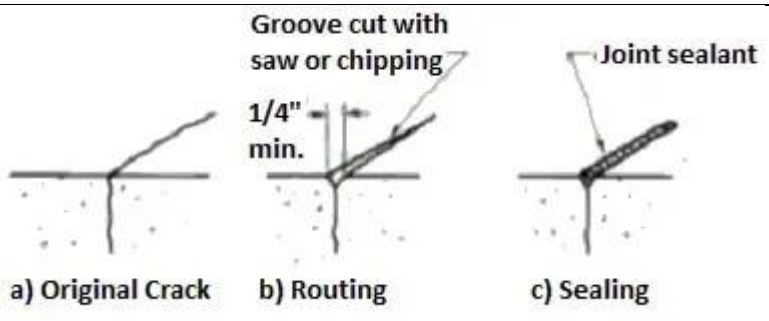

Figure 1.2. Routing and sealing of cracks**.**

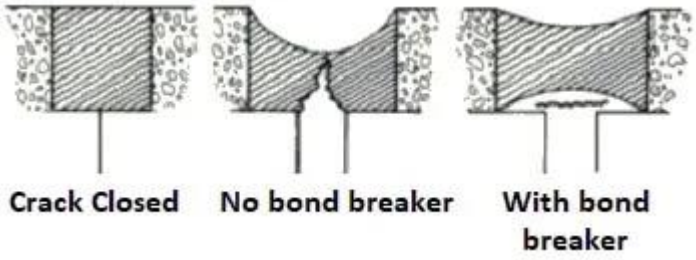

Figure 1.3: Concrete Crack with Bond Breaker

1.4.3 Concrete Crack Repair by Stitching

As shown in Fig. 1.5, stitching entails drilling holes on both sides of the fracture and grouting in U-shaped metal units with small staples or stitching dogs that cross the crack. If tensile strength is needed to be rebuilt across significant cracks, stitching may be used. Drilling holes on both sides of the crack, cleaning the holes, and anchoring the legs of the staples in the holes with either a non-shrink grout or an epoxy resin-based bonding solution are all part of the stitching technique.

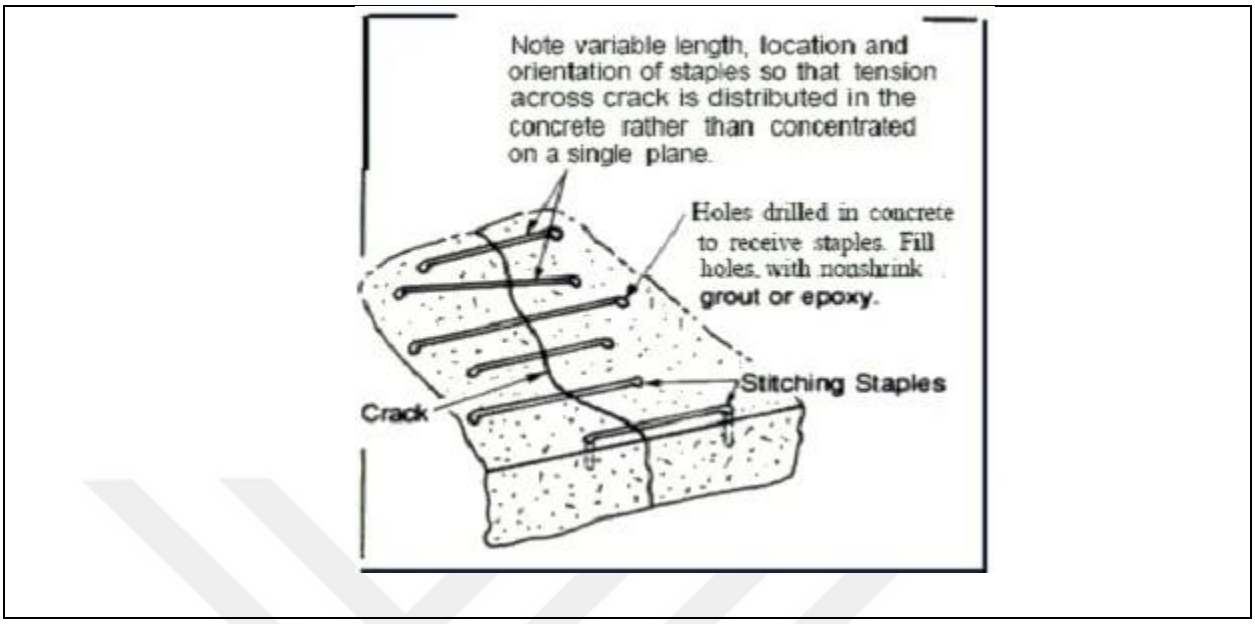

Figure 1.4: Concrete Crack Repair by Stitching

1.4.4 Utilization of FRP to repair and strengthening of the concrete beams

Nowadays with increasing the application of reinforced concrete beams in the structures and buildings [3-6], the usage of FRP materials to enhance the resistance to tensile stress and also repairing the cracked RCBs have been expanded, significantly [3, 5, 7-13]. Different types of FRP materials such as GFRP, CFRP, and BFRP can be utilized to improve the prevent crack propagation of the RCBs [14-22].

1.5 FINITE ELEMENT ANALYSIS

The FEM is a generic numerical method for solving partial differential equations with two or three variables in two or three dimensions (i.e., some boundary value problems). The FEM breaks a big system into smaller, simpler sections called finite elements in order to solve a problem. This is accomplished by a specific space discretization in the spatial dimensions, which is accomplished through the creation of a mesh of the object: the numerical domain for the solution, which has a finite number of points. A system of algebraic equations emerges from the finite element technique description of a boundary value issue. Over the domain, the approach approximates the unknown function. [23]. One of the main advantages of using finite element method and numerical analysis is decreasing the number of experiments. This critical advantage of the FEM method expanded the applications of simulations to predict the behavior of the structures and systems.

1.6 OBJECTIVES AND WORK PLAN

Reinforced concrete beams (RCBs) are widely used in the constructions due to their high strength and good flexural and compressive properties. However, low tensile strength of the concrete throughout flexural loading is the critical issue which limits their applications. Generally, cracks initiate from the bottom of the beams, where concrete is under the tension. Recently, researchers are using fiber reinforced polymers FRPs to enhance the strength of the beams and also repair the cracked zones of the RCBs. Fiber reinforced polymers materials have a wide use in a variety of applications, which are produced with a range of different stiffness and strength characteristics. Although, these materials share identical orthotropic properties and ductility. In contrast, the ordinary concrete is isotropic and brittle material.

Although, many experimental and numerical research have been conducted to investigate the effect of different types of FRPs on the flexural behavior of the beams, still there is a lack of information related to the impact of the reinforced thickness and shape of the FRFs on the crack propagation and deflection of the RCBs.

In the current thesis we are trying to investigate the effect of shape and different thickness of FRPs on the flexural properties of the RCBs using numerical methods by modelling the RCBs and FRP reinforcements in the ABAQUS software.

2. LITERATURE REVIEW

In this part of the thesis, first the theoretical foundations of deep beams reinforced with FRP are presented and then in order to get acquainted with the studies done on deep beams reinforced with FRP and to find the existing strengths and weaknesses, a number of researches done on FRP-reinforced deep beams are provided.

In the case of FRP-reinforced deep beams, there are generally no regulations that specifically address the FRP-reinforced deep beams. For ordinary beams in the existing relations of the regulations, the following expression is used to calculate the shear strength of the reinforced beam:

$$\boldsymbol{V_n = V_c + V_s + V_{frp}} \tag{2.1}$$

In this regard, V_c is the shear capacity of concrete (including the bearing share of concrete shear, the effect of grain lock and clamp and the lingual effect of beam flexural reinforcements), V_s is the shear strength of Stirrups and V_{frp} is the share of FRP materials in beam shear strength.

2.1 CHAALLAL MODEL

Chaallal et al. [24] proposed the following relation for V_{frp}, according to the structure of ACI 318-99:

$$\boldsymbol{V_{frp} = \emptyset_{frp} A_{frp} f_{frp} \frac{(\sin\beta + \cos\beta) d}{S_{frp}}} \tag{2.2}$$

In this relation, f_{frp} tensile strength of FRP materials and $\emptyset_{frp}$ reduction coefficient of resistance for FRP materials, A_{frp} cross section of a pair of FRP strips, β angle of the fibers to the horizon (clockwise), d effective beam depth and S_{frp} distance between FRP strips are along the axis of the beam. In addition, the average shear stress between the FRP material and the concrete intended for the design should not exceed half of the maximum adhesion stress.

This model has two main drawbacks:

a) It is assumed that all FRP materials cut by shear cracking have reached their maximum tensile strength, which is conservative in this assumption.
b) This modeling is not consistent with the experimental results in limiting the stress level in FRP materials that are likely to separate.

2.2 TRIANTAFILLOU MODEL

Triantafillou et al. [25] showed that it is almost impossible to accurately predict the contribution of FRP materials to the shear capacity of the beam. The criteria presented by him are based on European regulations.

$$V_{frp} = \frac{0.9}{\gamma_{frp}} E_{frp}\varepsilon_{frp}\rho_{frp}b_w d(1+\cos\beta)\sin\beta \quad (2.3)$$

In the relation above, E_{frp} is the coefficient of elasticity of FRP materials. Also, $\rho_{frp} = 2t_{frp}/b_w$, where t_{frp} is the thickness of the FRP layer, b_w is the width of the reinforced concrete beam and γ_{frp} is the partial safety factor for the tensile strength of FRP materials, the value of which is suggested for CFRP carbon reinforcement composites is 1.15.

The main weakness of this modeling is that no special difference is made for different shear reinforcement designs such as cross-section twisting and gluing to side surfaces as well as failure modes.

2.3 SMITH-TENG MODEL

Smith-Teng modeling was performed on the assumption that individual FRP strips could be equated with continuous plates. Therefore, these modelings can be used for both tape and FRP panels. Of course, for FRP tapes, there are some restrictions on the maximum distance between separate tapes. In a general reinforcement design, if the shear cracks are inclined at an inclination θ with respect to the longitudinal axis of the beam, the value of the share of FRP strips in the shear capacity of the beam is equal to:

$$V_{frp} = 2f_{frp}t_{frp}w_{frp}\frac{h_{frp}(\cot\theta+\cot\beta)\sin\beta}{S_{frp}} \quad (2.4)$$

In this regard, $f_{frp}$is the average stress in the FRP strip, below which a shear crack has passed in the final state. w_{frp} is the width of each of these strips, which is measured perpendicular to the position of the fibers in the strip. S_{frp}The horizontal distance of the strips from each other is β, the angle of inclination of the fibers, which is measured in a clockwise direction relative to the longitudinal axis of the beam on the left side of the fibers.

To investigate the shear behavior of FRP reinforced deep beams, Zhang et al. [26] tested 16 deep beams without steel shear reinforcement similar to Fig. 2.1. The FRP tape was attached to the beam at different angles and the beams were loaded to failure. The results indicate an improvement in the shear behavior of the beams and the amount of this increase depends on the placement of the jackets and their shape [26].

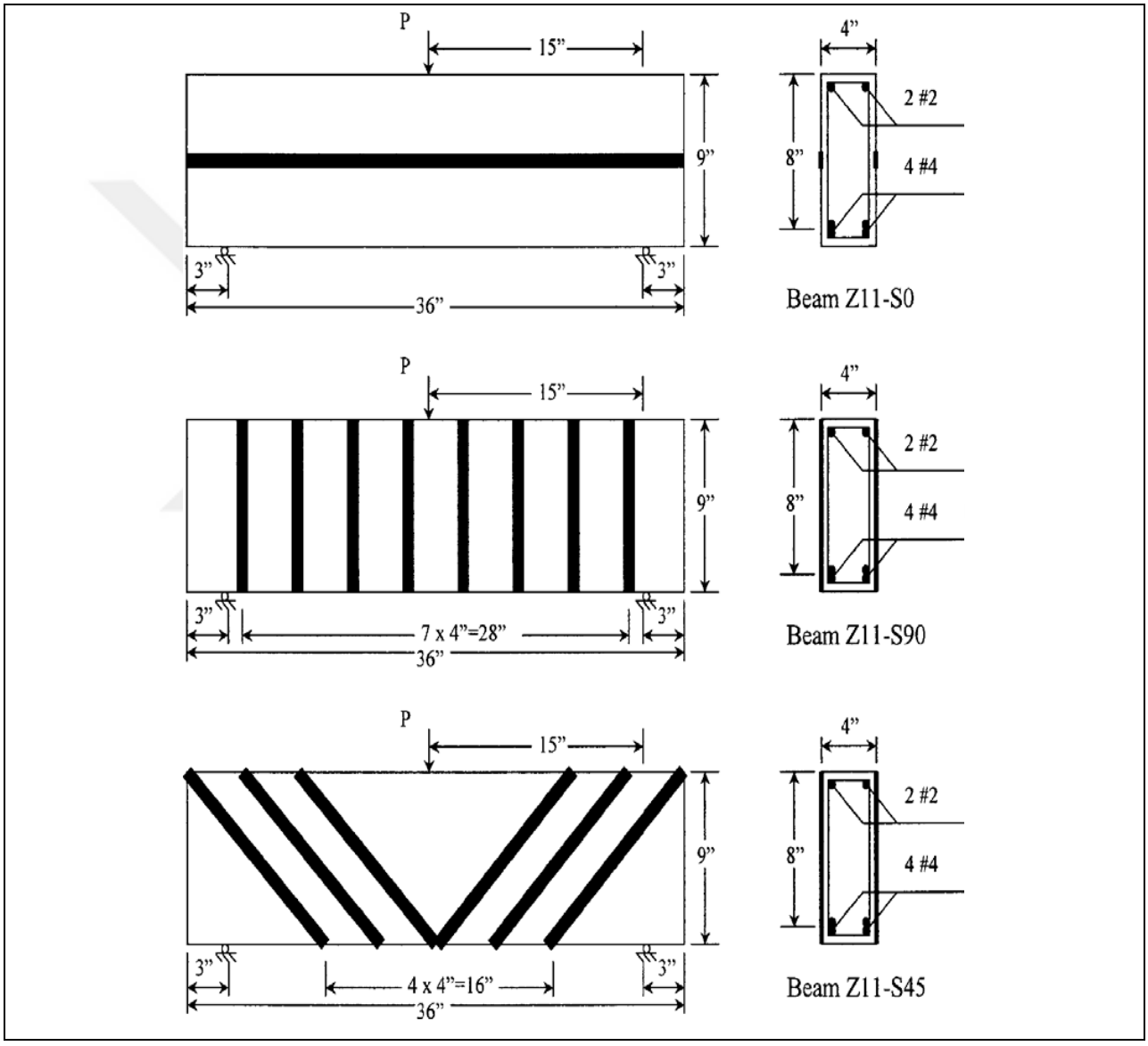

Figure 2.1: Three Types of Reinforce designed [26]

An analysis and design method for studying these beams based on Mau Soo [27] method was also proposed. According to Fig. 2.2, similar to the Mao and Su method, the shear stress V and the transverse compressive stress p of the shear element are borne by the reinforced steel, concrete and FRP reinforcements. When diagonal cracks form, the concrete compression handles are pressed and the steel rods and CFRP sheets act as clamps, forming a truss.

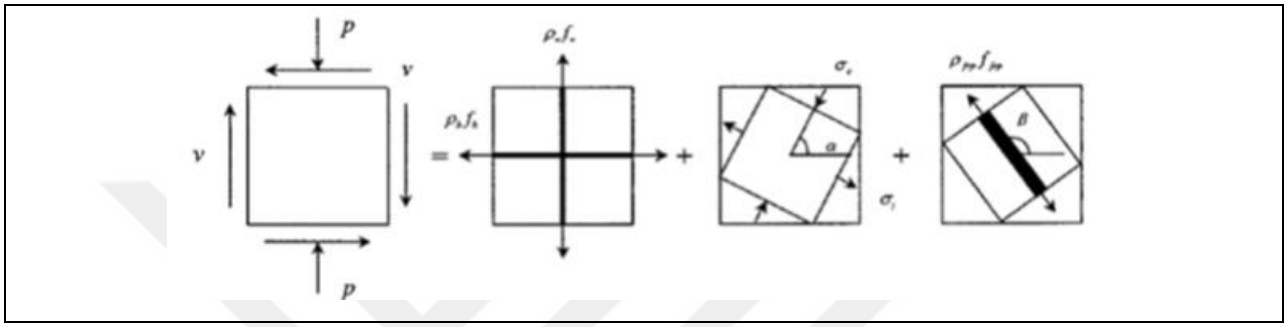

Figure 2.2: Stresses in the Shear Element [27]

The share of steel reinforcement along the vertical and horizontal is $\rho_v f_v$ and $\rho_h f_h$, respectively, where ρ_v and ρ_h are the ratio of vertical and horizontal steel reinforcement and f_v and f_h are the tensile strength of the reinforcement. Cracked concrete is considered. The stresses in cracked concrete can be shown to be perpendicular to each other with the principal compressive stress σ_c and the principal tensile stress σ_t. It should be noted that the tensile stress of concrete is very small. The share of CFRP reinforcement is equal to $\rho_{frp} f_{frp}$. Due to the fact that the tensile strength of CFRP materials is very high, the effective tensile stress is used and the failure mode of CFRP-reinforced beams is more in the form of detachment than fiber rupture in the ratio of steel reinforcement and CFRP is equal to:

$$\boldsymbol{\rho_v = \frac{A_v}{S_v b}} \tag{2.5}$$

$$\boldsymbol{\rho_h = \frac{A_h}{S_h b}} \tag{2.6}$$

$$\boldsymbol{\rho_{frp} = \frac{A_{frp}}{S_{frp} b} \sin \beta} \tag{2.7}$$

Considering the balance of the shear element by converting the main stresses of concrete and the tensile stress of CFRP along the longitudinal and vertical axes of the coordinates and the sum of the effects of tensile stresses of steel reinforcement, the following relations are obtained.

$$\sigma_c cos^2\alpha + \sigma_t sin^2\alpha + \rho_h f_h + \rho_{frp} f_{frp} cos^2\beta = 0 \tag{2.8}$$

$$\sigma_c cos^2\alpha + \sigma_c sin^2\alpha + \rho_v f_v + \rho_{frp} f_{frp} sin^2\beta = -p \tag{2.9}$$

$$(\sigma_c - \sigma_t)\cos\alpha \sin\alpha + \rho_{frp} f_{frp} \sin\beta \cos\beta = -1 \tag{2.10}$$

Finally, the shear strength was obtained from the following equation:

$$V = \frac{1}{2} b d_v f'_c \left[K(\omega_h + \omega_{frp} cos^2\beta) - \omega_{frp} \sin 2\beta\right] + \frac{1}{2} b d_v f'_c \sqrt{\left[K(\omega_h + \omega_{frp} cos^2\beta) - \omega_{frp} \sin 2\beta\right]^2 + 4\left[(\omega_v + \omega_{frp} sin^2\beta)(\omega_h + \omega_{frp} cos^2\beta) - \omega^2{}_{frp} \sin^2 2\beta \cos^2 2\beta\right]} \tag{2.11}$$

To investigate the effect of FRP on deep beams and also to find the type of optimal reinforcement, Islam and et al. [28] experimented on 6 deep beams reinforced with FRP. The beams tested had a lack of reinforcement from the beginning and one of the beams was reinforced without reinforcement as a control beam and the other beams were reinforced by jacket, tape and FRP mesh. Fig. 2.3 shows the geometric details of the beams. Dimensions and details of reinforcement of all beams are the same and are as follows:

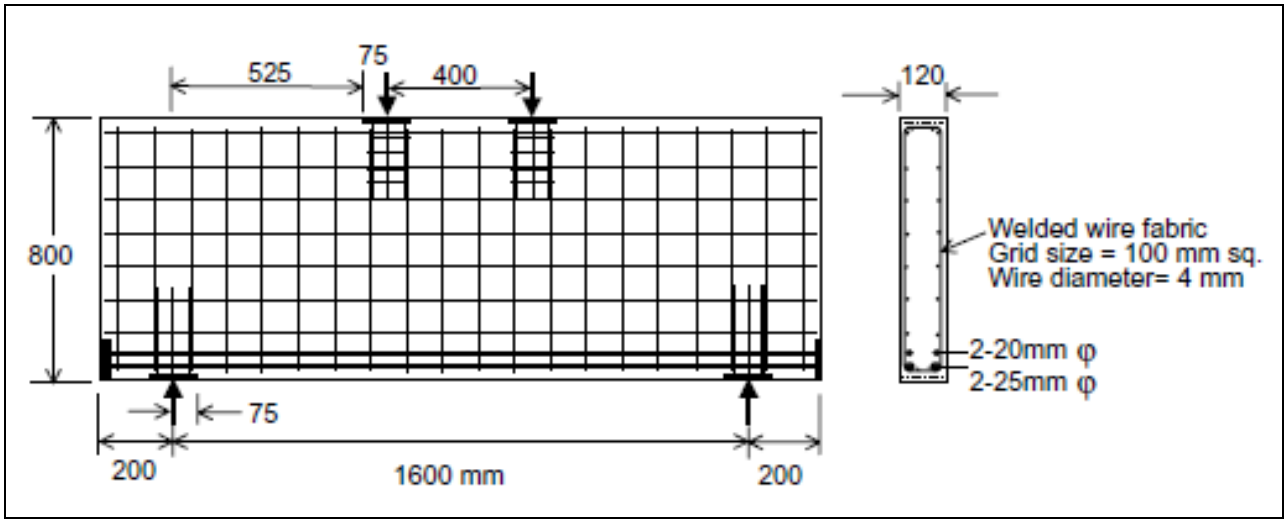

Figure 2.3: Geometrical properties of beams [28].

How to amplify the samples is shown in Fig. 2.4. The difference between networks 1, 2 and 3 in this figure is related to the cross-sectional area of the network.

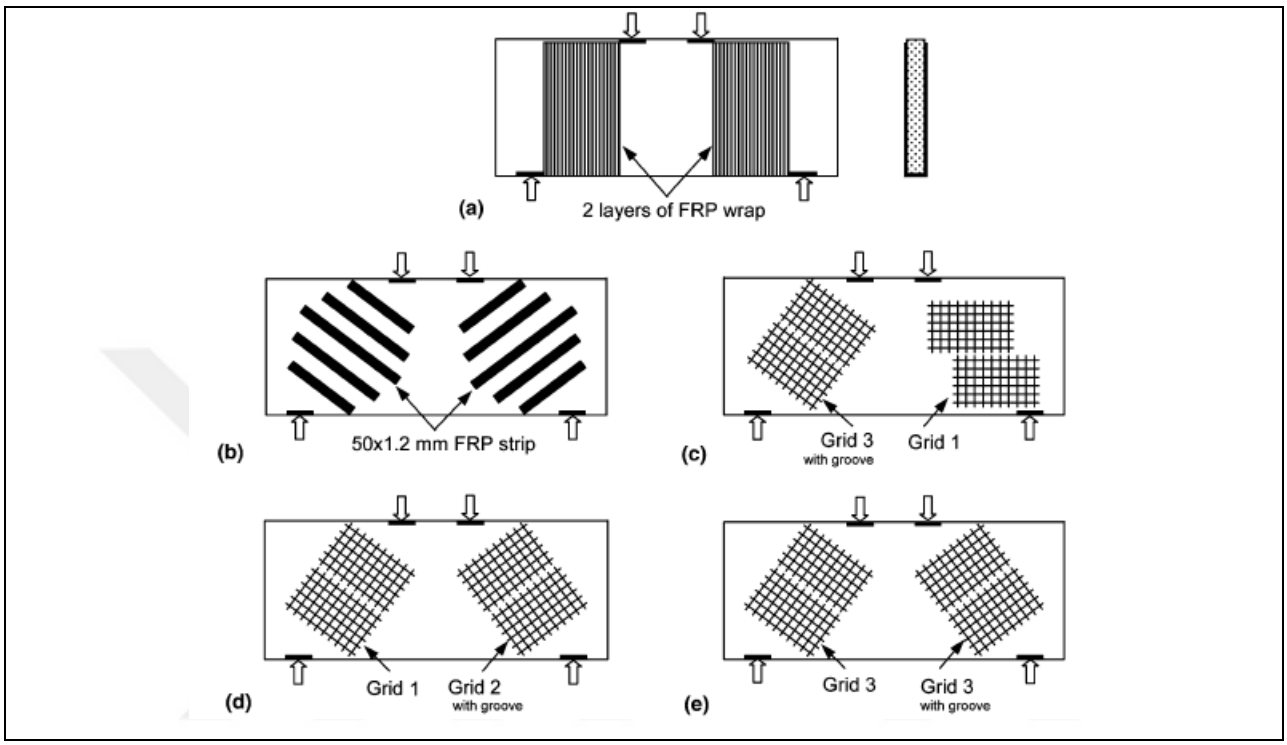

Figure 2.4: How the Beams are Reinforced [28].

The failure pattern of the beams was obtained by performing an experiment. As shown in Fig. 2.5, all the beams were damaged in the cut. The test results showed that the use of FRP mesh to strengthen the beams is more effective than a jacket or FRP tape.

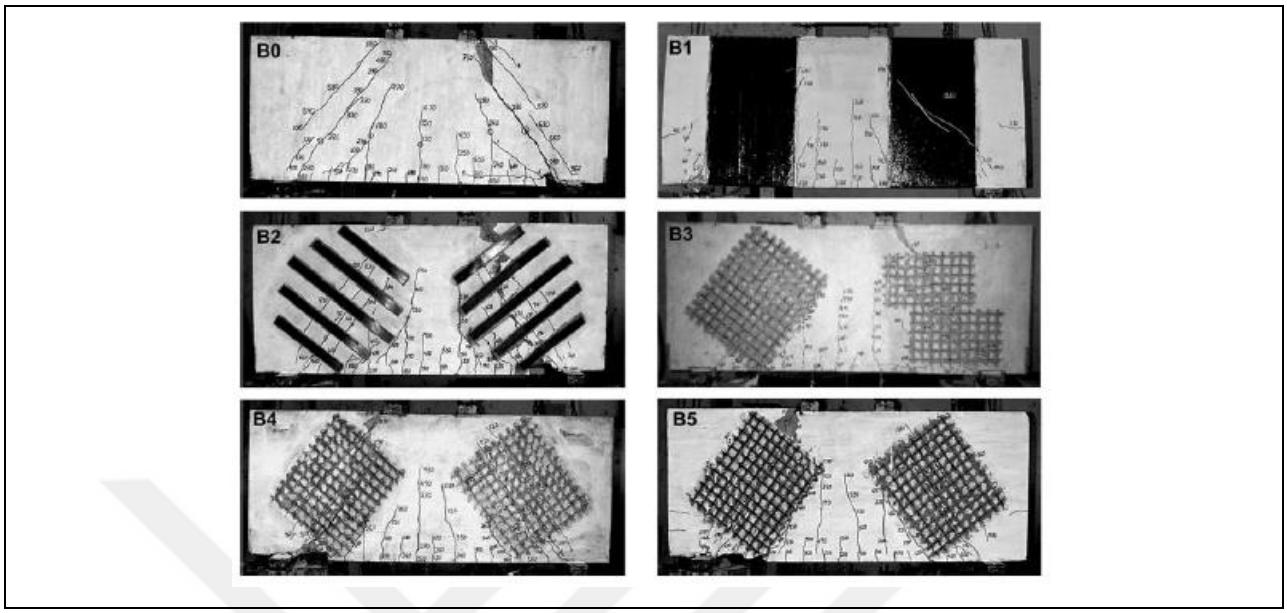

Figure 2.5: Beams Breaking Pattern

In a study by Ahmad et al. [29], they experimentally compared the behavior of short and deep beams made of concrete, reinforced with solid tubes of FRP (CFFT) polymer fibers, with their corresponding thin beams. 10 samples made of 4 types of FRP glass pipes with depth to cutout ratio between 0.9 to 6.25, thickness to diameter ratio between 16 to 23 and reinforcement index from 0.11 to 2.2 were tested under three- or four-point loads. The study of CFFT test specimens was continued to the lowest possible extent for the depth to shear ratio. Table 1 shows the details of the test beams.

Experiments showed that none of the tested CFFT beams break even under the cut to the lowest opening. Tensile flexural strain also remains at the bottom of the middle section of the beam, above the corresponding diagonal tensile strain in the middle of the shear opening. Also, shear cracks are observed only in the concrete core of CFFT deep beams with high reinforcement index and in the first bending crack, the concrete core starts to slip relative to FRP pipes. Finally, CFFT deep and short beams show a higher bending capacity than their corresponding thin beams, which are primarily due to members of the direct diagonal pressure and are developed in the intermediate core through an arc effect.

Table 2.1: The Experimental Sample Details (Ahmad et al, 2008)

Beam Type	Concrete Compressive Strength f_c' *(MPa*	a/D_j	Type Bonding Test	Span Length L(mm)	Reinforcement Index	Reinforcement Ratio ρ	D_e/t_j	Tube Thickness $t_j(mm)$	*Tube Outside Diameter* $D_e(mm)$	Beam No
Deep	40.7	0.9	Three point	579	0.11	6.3	63.1	*5.1*	*322*	S-1
Deep	40.7	1.0	Three point	338	0.14	8.1	49.2	*3.43*	*168.6*	S-2
Short	23.4	1.93	Four point	2286	0.22	7.2	55.9	*6.6*	*368.8*	S-3*
Short	31.0	2.0	Four point	1829	0.15	6.3	63.1	*5.1*	*322*	S-4
Deep	50.3	1.0	Three point	610	1.97	24.8	16.1	*19.0*	*305*	S-5
Short	29	2.04	Four point	2286	2.20	16.0	25.0	*13.9*	*347.7*	S-6*
Deep	66.9	1.0	Three point	640	0.24	8.9	44.9	*7.1*	*319*	S-7
Short	66.9	6.25	Four point	5500	0.24	8.9	44.9	*7.1*	*319*	S-8
Deep	40.7	1.0	Three point	653	0.51	8.8	45.3	*7.20*	*326*	S-9*
Short	60	6.14	Four point	5500	0.35	8.8	45.3	*7.20*	*326*	S-10*

The research conducted by Oman et al. [30] was related to the investigation of the shear behavior of short beams reinforced with FPR rebar without John reinforcement. For this purpose, 8 short beams reinforced with CFRP and 4 reinforced concrete beams reinforced with steel similar to Fig. 2.6 were tested. Only longitudinal tensile reinforcement was used to ensure shear failure in all beams and no die reinforcement was used. Crack pattern, reinforcement strain, failure mode, shear strength and drop of tested beams were studied. The effect of shear to effective depth ratio (a / d), effective beam depth, longitudinal reinforcement ratio and compressive strength of concrete on the shear behavior of CFRP-resistant deep beams was investigated. It was observed that the STM method can predict the shear strength of deep reinforced concrete beams compared to those reinforced with FRP and therefore need to be modified for FRP reinforced beams.

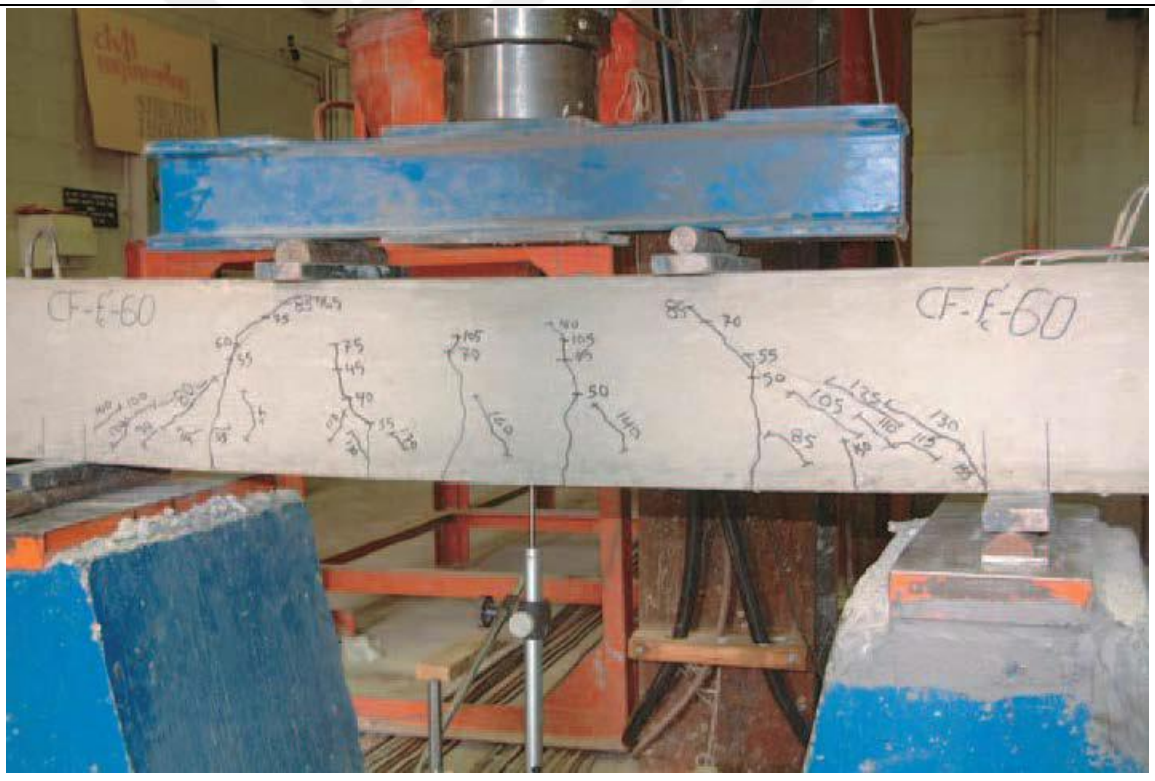

Figure 2.6: An Example of a Test Beam [30].

Park and Abutha [31] proposed the truss model (STM) for CFRP-resistant deep beams. In this study, they also examined seven calculated parameters to reduce the strength of cracked concrete. The STM model provides a simple and safe conceptual framework for investigating the load transfer mechanism in deep reinforced concrete members. This method is one of the design methods of reinforced concrete structures, which simplifies various types of complex concrete structures by converting complex stress states into a set of simple stress paths. The set of pressure handles, clamps and knots is called the truss model or mechanism. The proposed STM process begins with the selection of the truss model centerline and the attached CFRP strips as an additional tensile member in the STM model. This method is repeated until consistent geometric conditions and satisfactory results for the stress ratio of STM elements are obtained. Fig. 2.7 shows a simplified STM model.

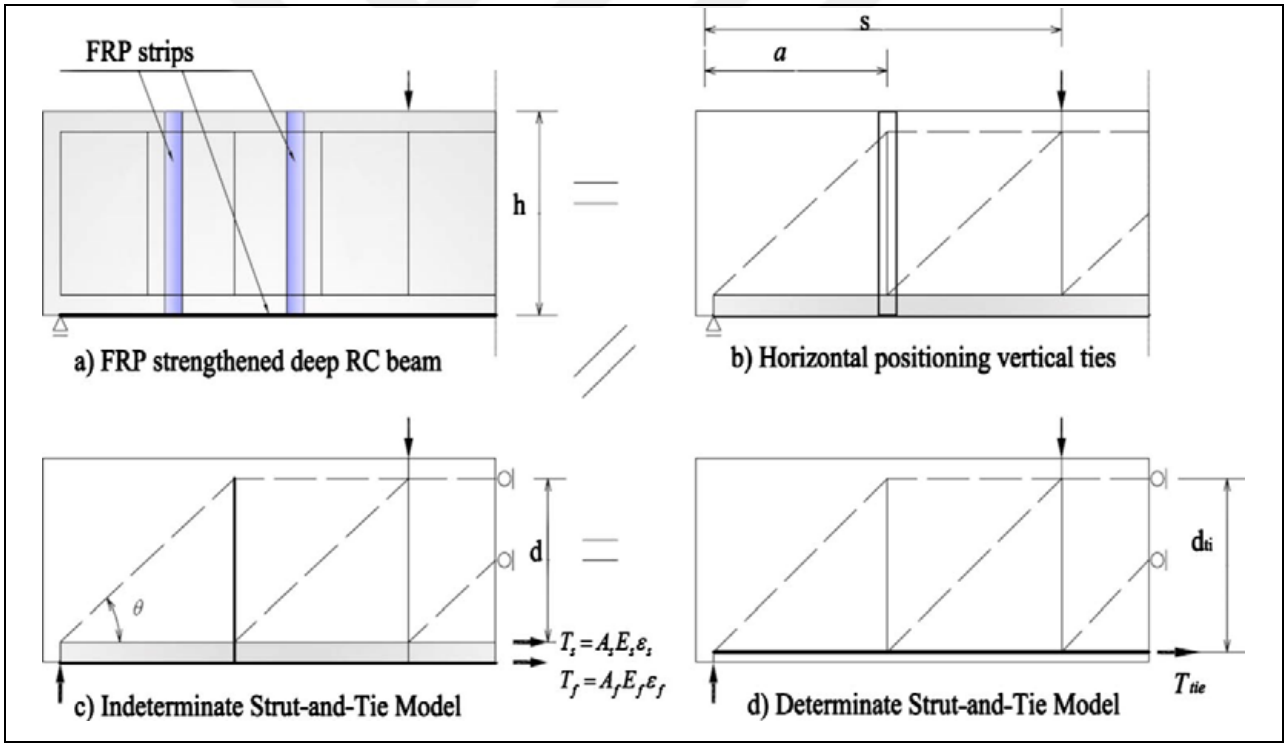

Figure 2.7: The Simplified Truss Model [31].

In calculating the tensile strength of the steel, the tensile strength of the steel was combined to a ratio of 1 and 0.75. The consideration of the CFRP force is due to the separation from the concrete before reaching the final strength. In this research, the results of 17-deep laboratory beam analysis are compared with the results of the proposed STM method. Table 2 shows this comparison. For

the proposed STM performance, effective models based on the shape of the pressure handles and concrete weight such as ACI 5-08, factor and effective model based on concrete strength such as Bergmeister et al. [31] and McGregor et al. [32] models have little agreement with the experimental results because these models have transverse stresses. Are not calculated in the direction of pressure grips in cracked concrete. But the effective factor model depends on the angle of the compression members such as Foster and Gilbert [33] Vecchio and Collins [34]. Like the LRFD and AASHTO models, they are in good agreement with the experimental results. The LRFD method downplays the strength of CFRP-reinforced deep concrete beams.

If effective models based on compression member angles or compression yield theory are used to calculate compressive members in cracked concrete, the proposed STM process provides a valuable analysis tool for CFRP-reinforced deep reinforced concrete structures.

Table 2.2: Comparing the experimental and STM method results [31].

LRFD	Foster and Gilbert	Vacchio and Collins	MacGreger	Bergmeister et al.	ACI	Test Result (kN)	Test Beams
17.14	7.94	7.94	7.94	7.94	30.95	63	REF
43.87	37.63	37.63	37.63	37.63	53.23	93	REF
17.65	13.44	10.43	25.28	-10.57	-6.59	132	FSI & FS2
26.70	22.95	20.28	-11.51	1.58	5.12	148.3	FSI & FS2
34.12	30.75	28.35	-0.22	11.55	17.73	165	FSI & FS2
34.52	31.17	28.78	0.38	12.08	15.24	166	FSI & FS2
25.71	20.23	17.87	-8.96	4.46	7.88	163	FS3
24.74	19.19	16.80	-10.4	3.21	6.68	160.9	FS3
40.37	32.58	32.85	34.33	35.40	37.65	115	SP1
39.63	32.02	32.02	33.52	34.60	36.88	113.6	SP1
37.99	30.18	30.18	31.71	32.83	35.17	110.6	SP2
38.22	30.43	30.43	31.96	33.07	35.41	111	SP2
33.42	25.02	25.02	26.67	27.87	30.39	103	SP3
37.65	29.79	29.79	31.34	32.46	34.82	110	SP3
22.68	12.70	12.70	14.96	16.75	19.05	137	FS
17.73	5.48	3.21	-32.5	-26.9	-25.1	142	RS
19.43	7.44	5.21	-29.8	-24.2	-22.5	145	RS

Maaddawy and Shrif [35] investigated the potential of using external bonding of carbon fiber composite sheets (CFRP) as an idea to increase the strength of deep-opening reinforced concrete beams. They also studied analytical methods for predicting the shear strength of deep reinforced concrete beams with openings reinforced with CFRP sheets. 13 deep beams were constructed and tested under four-point loading. Experimental specimens had a cross-sectional area of 80 × 500 mm and a length of 1200 mm. Of the two square openings, one was placed symmetrically in each shear opening. Experimental variables included opening size, position, and the presence of CFRP sheets. Fig. 2.8 shows the details of the test specimens and Figure 9 shows the details and location of the openings.

The results of this study were as follows:

a) The rupture state of deep unreinforced concrete beams with opening primarily depends on the size of opening, and the deep reinforced concrete beams with reinforcement in shear by CFRP with opening are suddenly ruptured due to the formation of diagonal shear cracks at the top and the depth of the opening.

b) CFRP shear reinforcement around openings in deep reinforced concrete beams significantly increases beam strength as well as stiffness when openings are in the middle of the shear opening. The strength obtained by CFRP sheets is in the range of 35-73%.

c) Comparison between experimental and analytical results showed that the analytical method can provide a more reasonable prediction for the shear strength of deep reinforced concrete beams with opening and reinforced by CFRP.

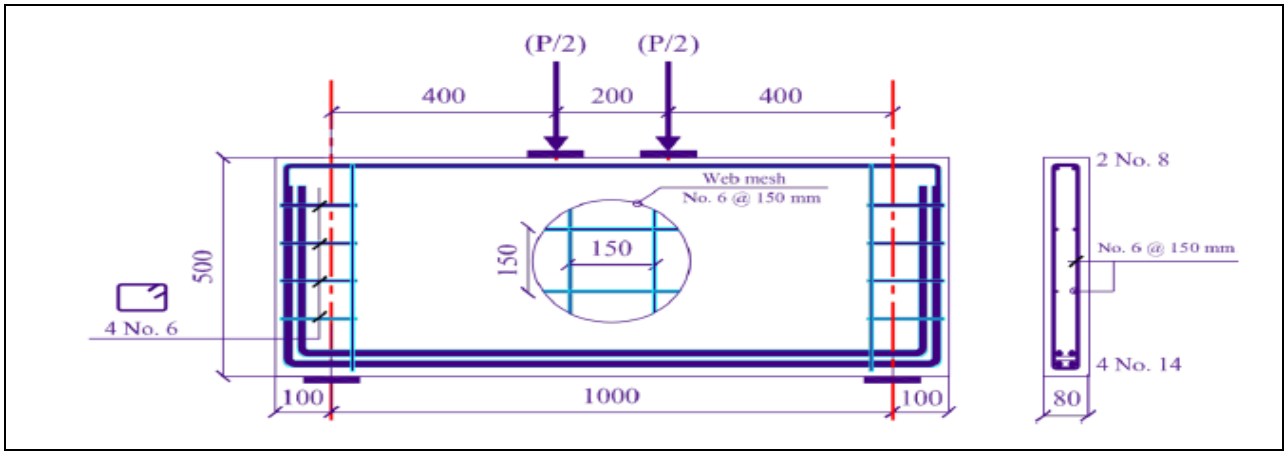

Figure 2.8: Details of Experimental samples [35].

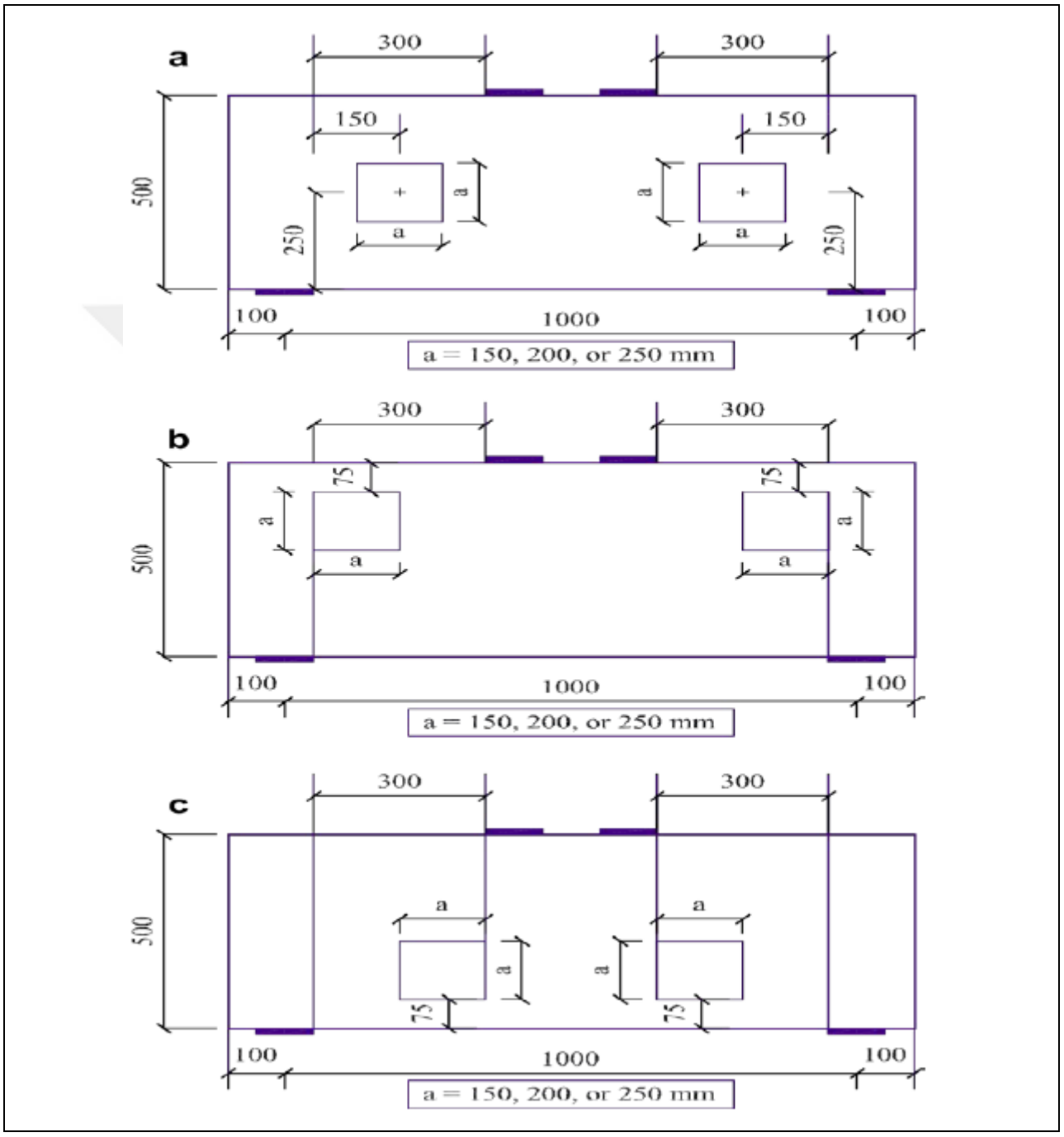

Figure 2.9: Detail and the Location of Openings [35].

In a dissertation at the University of Alberta, Andermatt investigated the shear behavior of deep reinforced concrete beams reinforced with FRP rebar without reinforcement. Experimental results of 12 large-scale samples were reported [36]. The main variables included a / d ratio, reinforcement ratio, member height and concrete strength. After testing, it was found that for all types of reinforcement, an increase in the ratio of increase in (a/d) reduces the shear strength.

Also, the ratio of reinforcement, regardless of its type, is proportional to the shear strength. Figure 10 shows the details of the samples. The specimens were named under three characteristics, the letters C B A indicating the total height of the specimens (specimen A is 300 mm high, B is 600 mm high and C is 1000 mm high). After these letters, in order of increasing the size of the samples, a number is placed from 1 to 6, and at the end, one of the letters H is written to mean high-strength concrete or N means ordinary concrete.

The results showed that the arc mechanism of forming in reinforced concrete beams with FRP, with the ratio of a/b < 2.1 in the STM process accepted by CSA A23.3-04 is able to accurately predict the capacity of reinforced beams with FRP rebar.

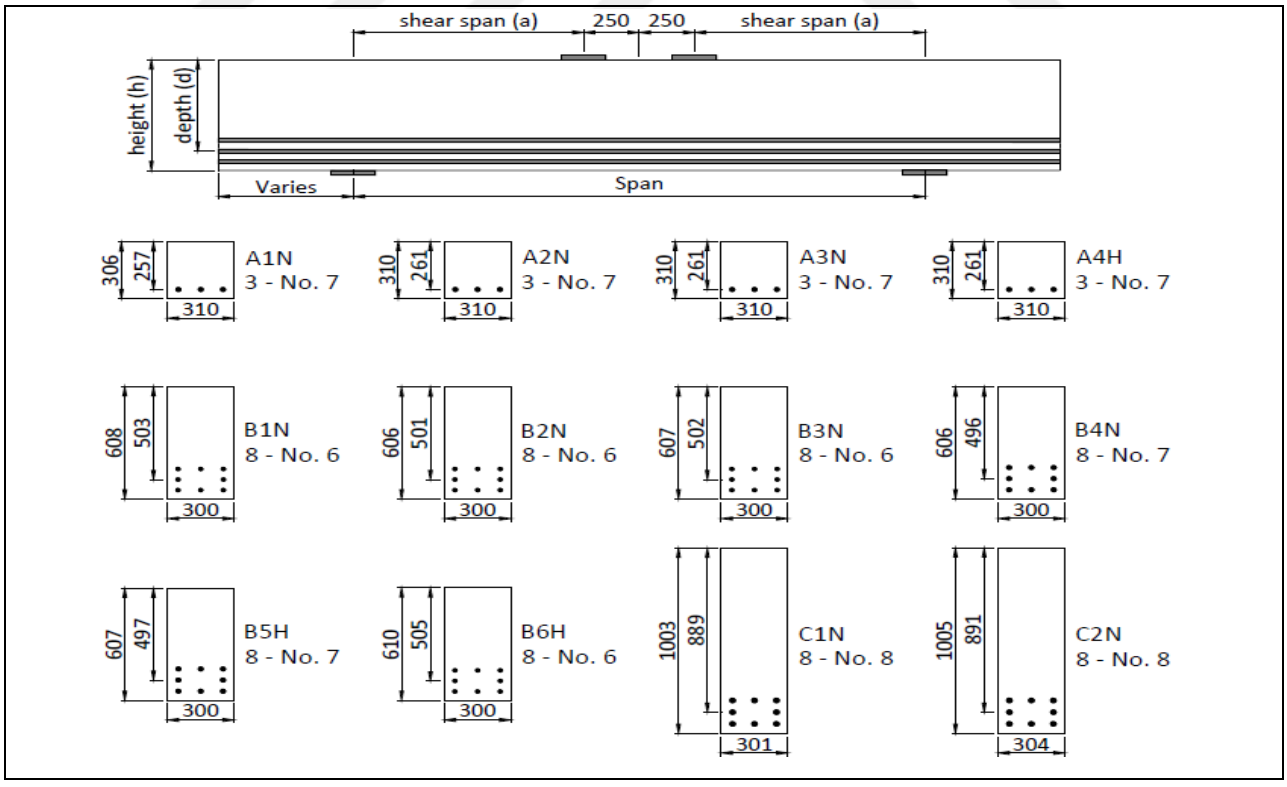

Figure 2.10: Details of Samples [36].

Lee et al. [37] investigated the behavior of resistant T-beam deep beams with CFRP sheets. 14 deep T-shaped beams similar to Fig. 2.11 that were deficient in cutting were considered with an opening-to-effective ratio of 1.22. The following figure shows the dimensions and cross-sectional details of the beams.

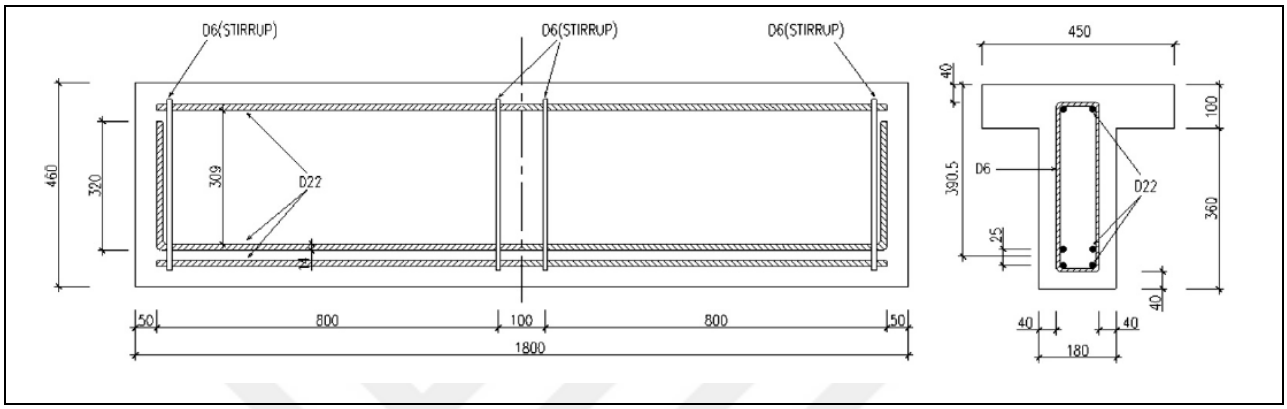

Figure 2.11: Details of Beam Reinforcement [37].

Important Parameters of Resistance Length and Composition of CFRP Sheet Fiber were studied. The two layers of FRP sheet with lengths of one-fourth, one-half and one-half shear openings were used, with the length of the fibers of each layer with the other layer being 0/0, 90/90, 0 / 90, 45/135 degrees. An example of a beam is shown in Fig. 2.12.

Figure 2.12: An Example of Reinforced Beams [37].

Table 3 shows how to strengthen and angle the fibers for each beam. One of the beams was unreinforced and the other was reinforced with U-shaped FRP. The rest of the beams were reinforced with FRP only in the John area and on both sides of the beam.

Table 2.3: Properties of Reinforcement of Samples [37].

Fiber direction combination	Strengthening length	Strengthening configuration	Designation
	Quarter length of shear span	Side only	CT
$0^{\circ}/0^{\circ}$	Quarter length of shear span	Side only	CS-QL-HP
$90^{\circ}/90^{\circ}$	Quarter length of shear span	Side only	CS-QL-VP
$90^{\circ}/0^{\circ}$	Quarter length of shear span	Side only	CS-QL-CP
$45^{\circ}/135^{\circ}(135^{\circ}/45^{\circ})$	Half-length of shear span	Side only	CS-QL-AP
$0^{\circ}/0^{\circ}$	Half-length of shear span	Side only	CS-HL-HP
$90^{\circ}/90^{\circ}$	Half-length of shear span	Side only	CS-HL-VP
$90^{\circ}/0^{\circ}$	Half-length of shear span	Side only	CS-HL-CP
$45^{\circ}/135^{\circ}(135^{\circ}/45^{\circ})$	Full of shear span	Side only	CS-HL-AP
$0^{\circ}/0^{\circ}$	Full of shear span	Side only	CS-FL-HP
$90^{\circ}/90^{\circ}$	Full of shear span	Side only	CS-FL-VP
$90^{\circ}/0^{\circ}$	Full of shear span	Side only	CS-FL-CP
$45^{\circ}/135^{\circ}(135^{\circ}/45^{\circ})$	Full of shear span	Side only	CS-FL-AP
$90^{\circ}/0^{\circ}$	Full of shear span	U-wrap	CSU-FL-CP

Table 2.4 shows the test results. Almost all specimens except CS-FL-HP showed shear-compressive failure due to lamination of CFRP sheets. The effects of key variables on the shear performance of reinforced deep beams were determined from the load-displacement curve.

Table 2.4: Results of testing samples [37].

Ultimate Loa d (kN)	Cracking loads(kN)		Specimen
	Shear	Flexure	
	161.8	55.9	CT
$0^{\circ}/0^{\circ}$	222.6	68.6	CS-QL-HP
$90^{\circ}/90^{\circ}$	222.1	80.2	CS-QL-VP
$90^{\circ}/0^{\circ}$	321.4	60.8	CS-QL-CP
$45^{\circ}/135^{\circ}(135^{\circ}/45^{\circ})$	224.6	76.5	CS-QL-AP
$0^{\circ}/0^{\circ}$	333.4	68.8	CS-HL-HP
$90^{\circ}/90^{\circ}$	286.4	82.4	CS-HL-VP
$90^{\circ}/0^{\circ}$	318.7	85.3	CS-HL-CP
$45^{\circ}/135^{\circ}(135^{\circ}/45^{\circ})$	323.6	78.5	CS-HL-AP
$0^{\circ}/0^{\circ}$	-	78.6	CS-FL-HP
$90^{\circ}/90^{\circ}$	-	76.5	CS-FL-VP
$90^{\circ}/0^{\circ}$	-	78.5	CS-FL-CP
$45^{\circ}/135^{\circ}(135^{\circ}/45^{\circ})$	-	107.9	CS-FL-AP
$90^{\circ}/0^{\circ}$	-	103.0	CSU-FL-CP

3. NUMERICAL SIMULATION

In this thesis, ABAQUS V6.21 was utilized to simulate all the conditions and numerically analyze them. ABAQUS is a famous finite element software which is very user friendly, and it can be employed for analyzing an extensive linear and non-linear model. Various mechanical properties such as elastic modulus, stress-strain, density, damage criteria include Hashin and inelastic damages for steel, concrete and FRP materials were defined in property section of ABAQUS. It is worth noting that the damage criteria for all materials were performed using concrete damage plasticity (CDP) model. For all loading sections include elastic region and plastic region isotropic damaged plasticity theory is used [38]. The CDP model and related parameters are shown in Table 3.1.

The experimental results from the literature were used to identify both compressive and tensile stress vs strain chart of the concrete for the simulation. The relevant formula for compression and tension are listed below, respectively. It must be noted that these relationships are credential for the uniaxial loading.

$$\sigma_c = E_0\,(1 - d_c)\left(\varepsilon_c - \varepsilon_c^{pl}\right) \tag{1}$$

$$\sigma_t = E_0\,(1 - d_t)\left(\varepsilon_t - \varepsilon_t^{pl}\right) \tag{2}$$

Where in these formulas σ_c, d_c, E_0, are the compressive stress, compressive damage variable and the elastic modulus of the concrete, separately. Furthermore, for the second equation, σ_t, d_t, E_0, are tensile stress, tensile damage variable, correspondingly. Moreover, ε_c is compressive strain and ε_c^{pl} is compressive plastic strain, respectively. Lastly, ε_t and ε_t^{pl} are the strain under the tension and tensile plastic strain, respectively.

Table 3.1. CDP parameters of Concrete [39].

Dilation Angle (Ψ)	Eccentricity (Є)	fb_0/fc_0	K	Viscosity (μ)
56	0.1	1.16	0.667	0.0001

On the other hand, another model progressed by Lubliner et al. [40] was performed in ABAQUS to simulate the failure of the concrete. The aforementioned model has been modified by different investigators [39]. The mechanical properties in plastic regions must be explained using the different phenomena such as deterioration of material strain softening and hardening as well as volumetric expansion which subsequently decreases stiffness and strength of concrete. furthermore the extensive information and other theories related to CDP model can be found in ABAQUS Analysis User's Manual [41].

Furthermore, the plastic behavior for strain and stress throughout the damage of concrete can be attained by the Equations (3) and (4). Also, the degradation can be happened in the softening section where stiffness is relational to the cohesion of the beam.

$$\frac{E}{E_0} = \frac{C}{C_{max}} = (1 - d) \tag{3}$$

$$\varepsilon^{-p} = \varepsilon^{p} - \frac{d}{1-d}\frac{\sigma}{E_0} \text{ and } \varepsilon^{-p} = \varepsilon - \frac{f}{E_0} \tag{4}$$

In above equations C is cohesion, which is also proportional to stress, C_{max} represents the concrete's strength, and also, d and f are damage parameter and the compressive or tensil strength of concrete. Moreover, damage compression for model elements and tensile parameters are determined by Equations (5) and (6), independently.

$$d_c = 1 - \frac{\sigma_C E_C^{-1}}{\varepsilon_c^{pl}\left(\frac{1}{bc} - 1\right) + \sigma_c E_C^{-1}} \tag{5}$$

$$d_t = 1 - \frac{\sigma_t E_C^{-1}}{\varepsilon_t^{pl}\left(\frac{1}{bt} - 1\right) + \sigma_t E_C^{-1}} \tag{6}$$

Which σ_c is the stress in the compression mode, and σ_t is stress in the tension mode. E_c is the concrete modulus elasticity, ε_t^{pl} is the plastic part of the strain. The parameters include of b_c and b_t are suggested by [42] and which are set as 0.7 and 0.1, respectively.

The cracks under the reinforced concrete beams which happening when the beam is under the flexural loading and bending, are the most common types of cracks. These cracks initiate in the bottom part of the beam and propagate through the central regions and subsequently cause the

failure of the beam. The reason that these cracks starts from the bottom of the beam is low tensile strength of the concrete and the tension appears at the bottom part of the beam when it is under the flexural loading. Therefore, flexural loading was used in the current thesis to observe the behavior of reinforced beam after initiation of the cracks.

In this thesis four-point bending experiments were numerically analyzed and simulated in ABAQUS, where the schematic of the reinforced concrete beam with embedded steel bars and stirrups are shown in Fig. 3.1. Th dimensions of the beam have been shown in the figure where width, height and length were chosen based on the consistency with the other experimental and numerical works as 300 mm, 200mm, and 2400 mm, respectively.

Furthermore, as it is mentioned in the schematic, the beam has been reinforced using four long bars which the diameters of them are 8 mm and series of stirrups via an interval spacing of 0.1 m c/c (Shown in Fig. 3.1). The elastic modulus of the commercial steel for different parts of the reinforcements such as bars and stirrups has been chosen and stated as 200 GPa. Moreover, other mechanical properties of the elements were defined and written in ABAQUS to provide the necessary information for the analysis. Also, compressive strength (fc) of the concrete employed in this thesis was 30 MPa.

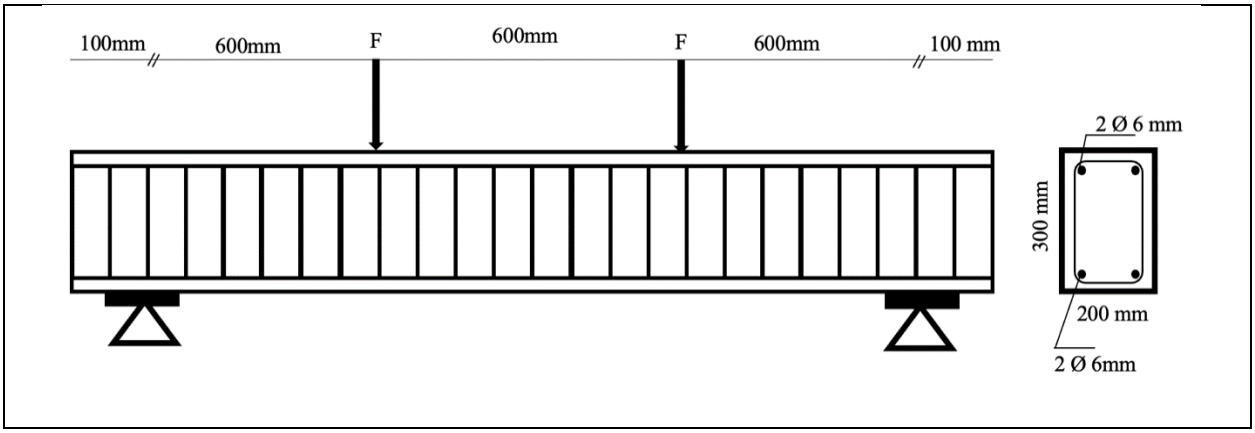

Figure 3.1: Schematic of reinforced concrete beam under the four-point bending experiment with the dimensions of the bars and stirrups inside the beam.

Based on the experimental results mechanical properties of the concrete which has used in the simulation is listed below in Table 3.2. Two different criteria have been considered to achieve the best results in numerical modeling. The first one was concrete damage plasticity (CDP) which is important when we want to investigate the damage behavior of structure after yield point to see the behavior of the plastic region and crack initiation and propagation. Also, the other important criteria are dynamic mechanical behavior of the concrete which is very crucial to predict the behavior of the concrete based structured after applying flexural load on them. The Dynamic behavior of concrete utilized for the numerical analysis as well as damage behavior employed in ABAQUS is shown in Table 3.2.

Table 3.2: Dynamic Mechanical Properties and Tensile Damage behavior of concrete.

Tensile (CDP)				Tensile Damage	
stress	in-strain	stress		damage	in-strain
3450652.112	0	3450652		0	0
2295713.038	0.00029	2295713		0.740058	0.00029
1884035.156	0.000549	1884035		0.868129	0.000549
1651583.006	0.000802	1651583		0.916419	0.000802
1496056.714	0.001052	1496057		0.940729	0.001052
1382096.603	0.0013	1382097		0.955019	0.0013

3.1 MECHANICAL MODELING

In this section, different steps of the modelling, definition of the parts, interactions and meshing have been mentioned and explained, briefly. Primarily, Fig. 3.2 shows the environment of ABAQUS when we want to model the structure and analyze it. As it can be seen in the figure, there are different modules in ABAQUS software which help the user to define, model, mesh, and then analyze the structure. These modules are listed as part, property, assembly, interaction, load, mesh, optimization, job, visualization, and sketch. All the operations and modifications for this simulation in each step are explained briefly in the current section of the thesis.

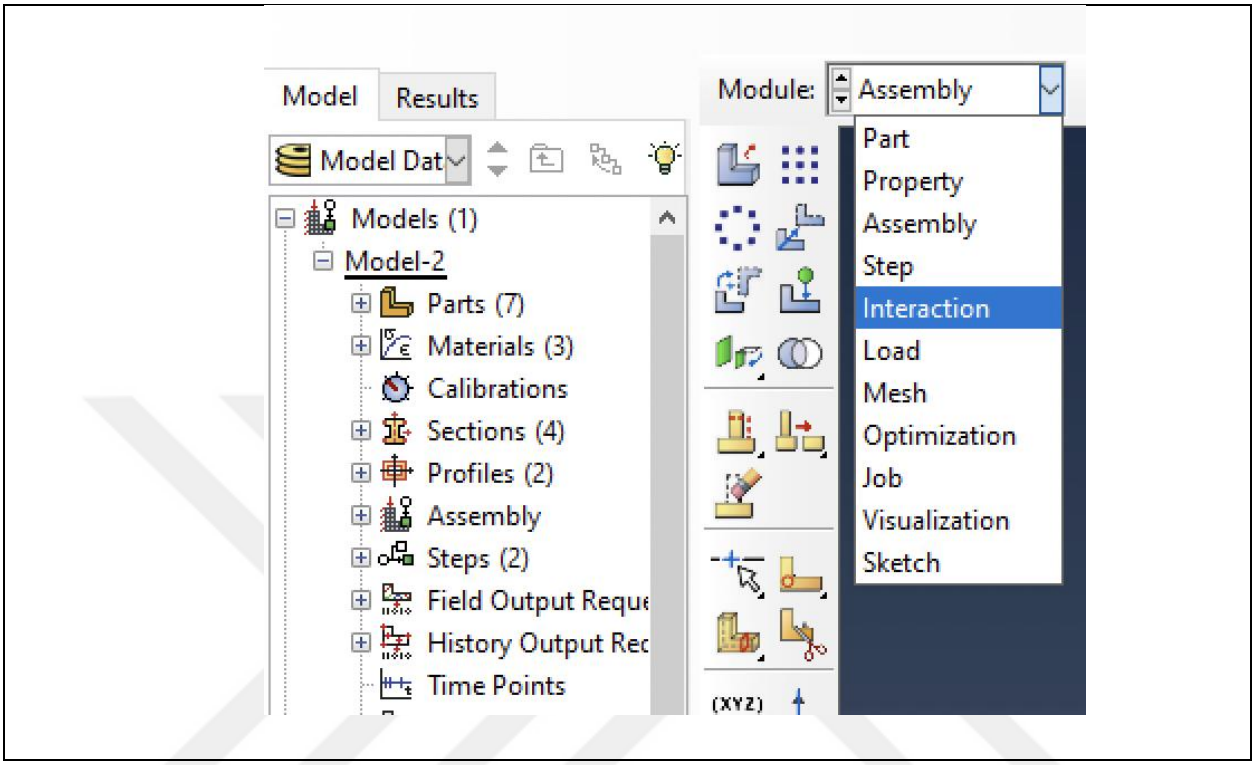

Figure 3.2: Module Bar of ABAQUS

3.1.1 Part Module

In the part module all the parts of the setup such as beam steel reinforcements (bars and stirrups), FRP laminated layer, hydraulic jacks, and supports. Fig. 3.3 shows the complete embedded region includes 20 series of stirrups with 4 long bars attached inside the rectangular stirrups. Moreover, in order to simulate hydraulic jack loading from the top side of the beam two rigid bodies have been designed to apply the load on four-point bending system. Also, two support have been put in both side of the reinforced concrete beam and the movement of these two rigid parts were limited to be fixed at both sides (See Fig. 3.3).

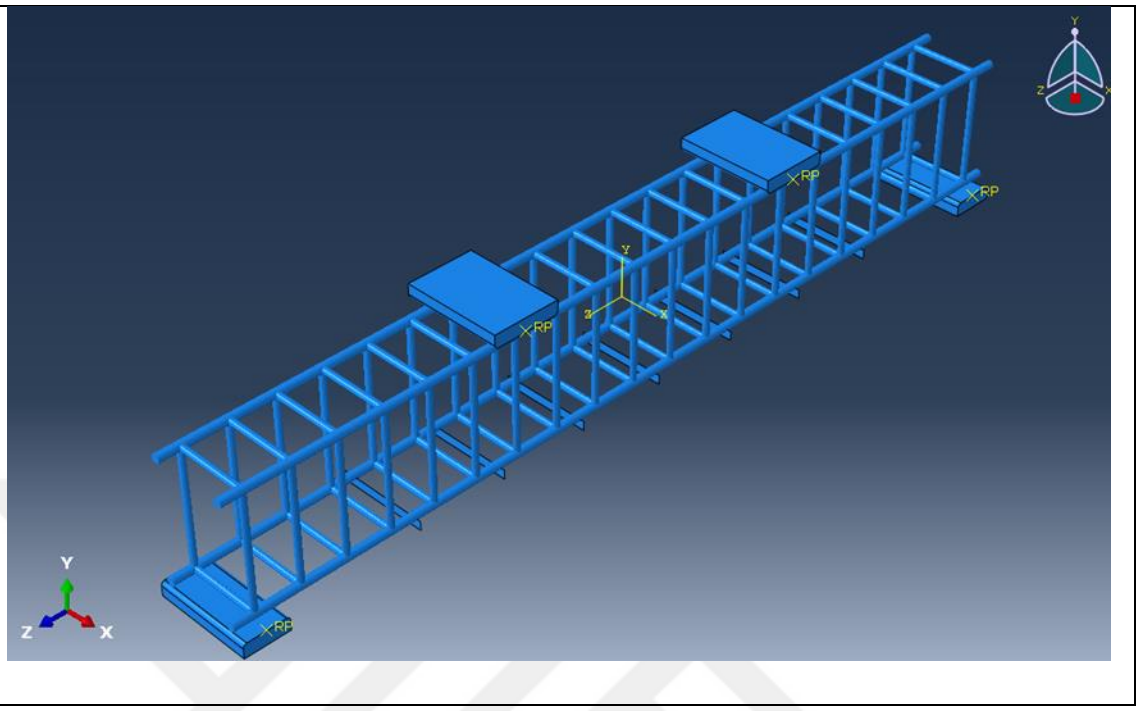

Figure 3.3: Embedded Stirrups and Bars of Steel

Also, as it can be seen in Fig. 3.3, seven cracks have been designed in order to define the pre-cracked version of the beam. Subsequently, wrapped FRP was designed to cover the bottom and sides pf the beam to strengthen the pre-cracked reinforced concrete beam. The schematic of this wrapped layer is demonstrated in Fig. 3.4. The wrapped version of CFRP was used also to compare the flexural strength but the main focus of this work was on the laminate CFRP layer in the bottom part of RCB.

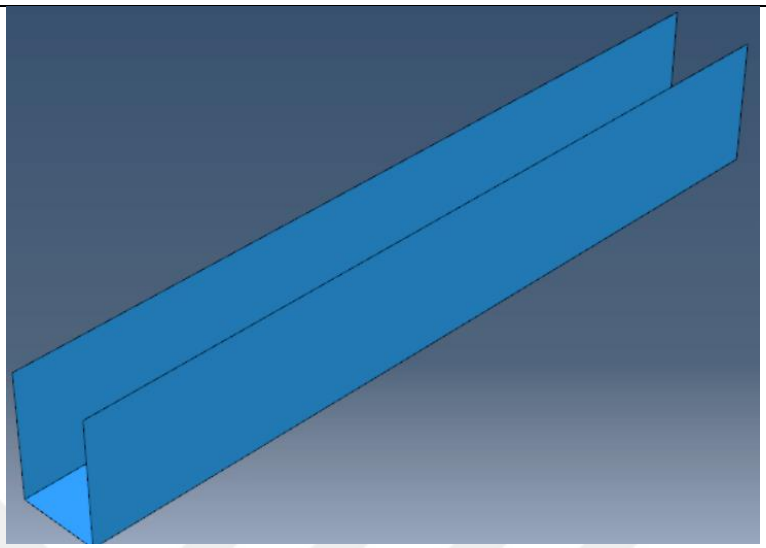

Figure 3.4: The Schematic of Wrapped FRP.

3.1.2 Mesh Module

For the next part of the modelling in ABAQUS, the interactions between different parts of the system and constraints and contacts were defined. Afterward, in mesh module all the parts were meshed one by one to discretize the parts for numerical solution. Although, low element size may give better results, the low element size increases the number of the elements which subsequently increase the simulation time. Therefore, we have tried to optimize the number of the elements and element size to achieve a reliable result and compute the problem faster. In most of the cases of this thesis, the approximate global size was defined as 0.05. Fig 3.5 demonstrates the system for the four-point bending test after mesh. Also, the FRP laminate was shown in Fig. 3.6.

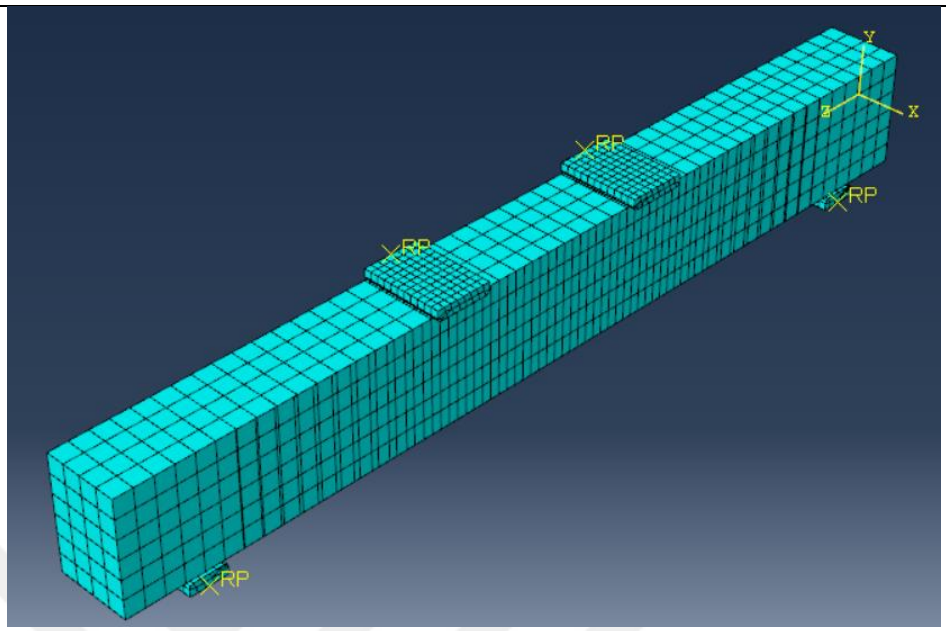

Figure 3.5: Meshed Setup.

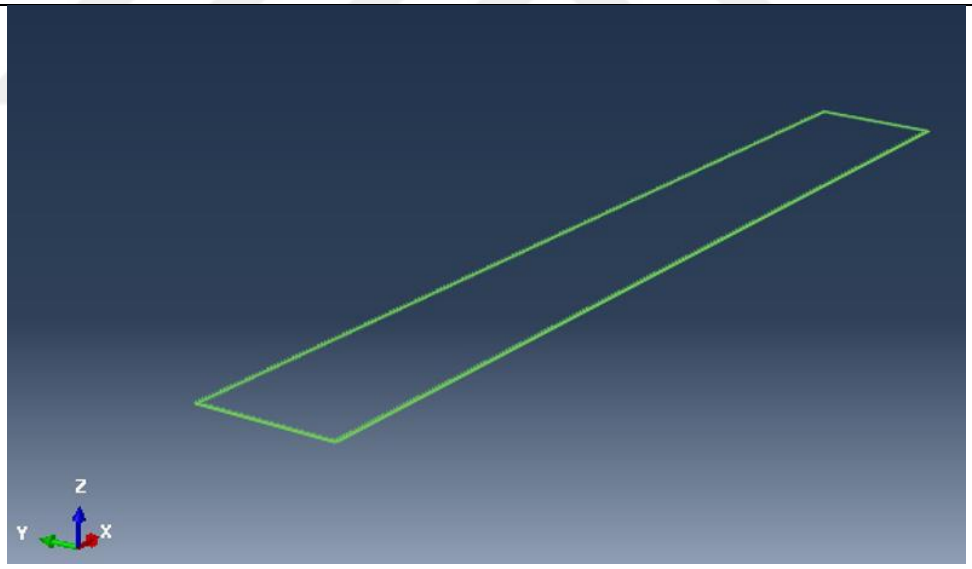

Figure 3.6: FRP Laminate (Different sizes have been used).

In Abaqus software, three types of cracks can be modeled to consider material failure, which should be defined in the material properties section.

3.1.3 Material Property Module

In this part all the sections that have been defined, must be well-explained in terms of the mechanical and structural properties in order to import all the specifications that software needs to be able to complete the analysis of the setup. Three main sections of steel reinforcements, concrete beam, and FRP material must be identified in terms of mechanical properties. In Fig. 3.7. the material manager window can be seen that three main materials of the simulation have been defined in that.

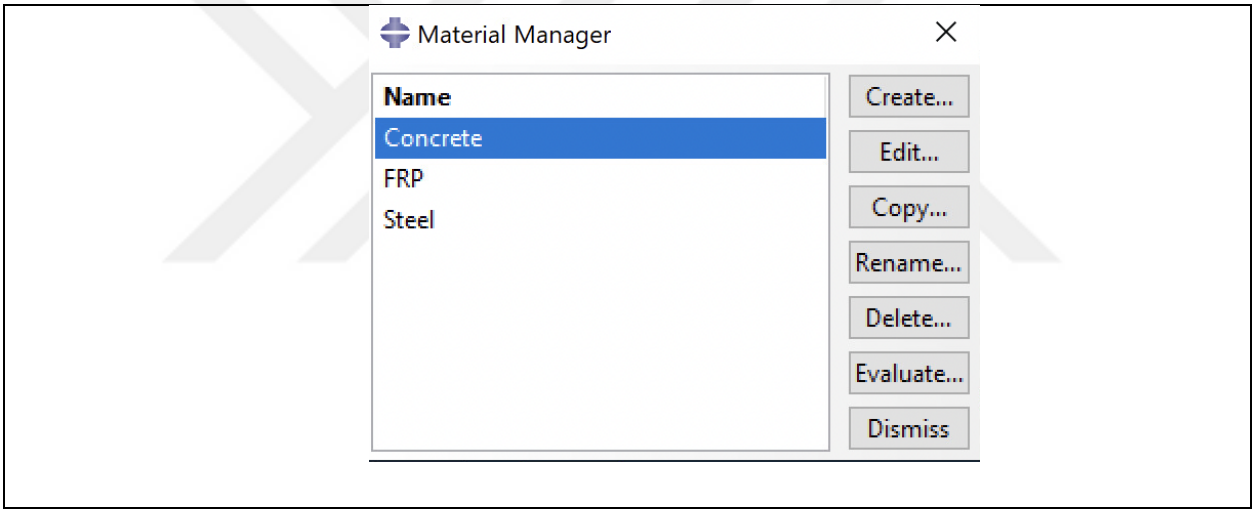

Figure 3.7: Material Manager Window of the ABAQUS.

As shown in Fig. 3.8, the material properties for concrete have been defined such as maximum Principal damage, damage evolution, density, elastic, and concrete damaged plasticity. These properties are needed in order to define the failure of the concrete after applying the flexural load on that. The maximum principal stress to start cracking and damage of the concrete was set as 2 MPa based on the other experimental works where they have shown that the concrete can start and initiate cracks after reach to 2 MPa. This crack initiation happens at the middle bottom part of the beam where the tension is at the highest level throughout the reinforced concrete beam.

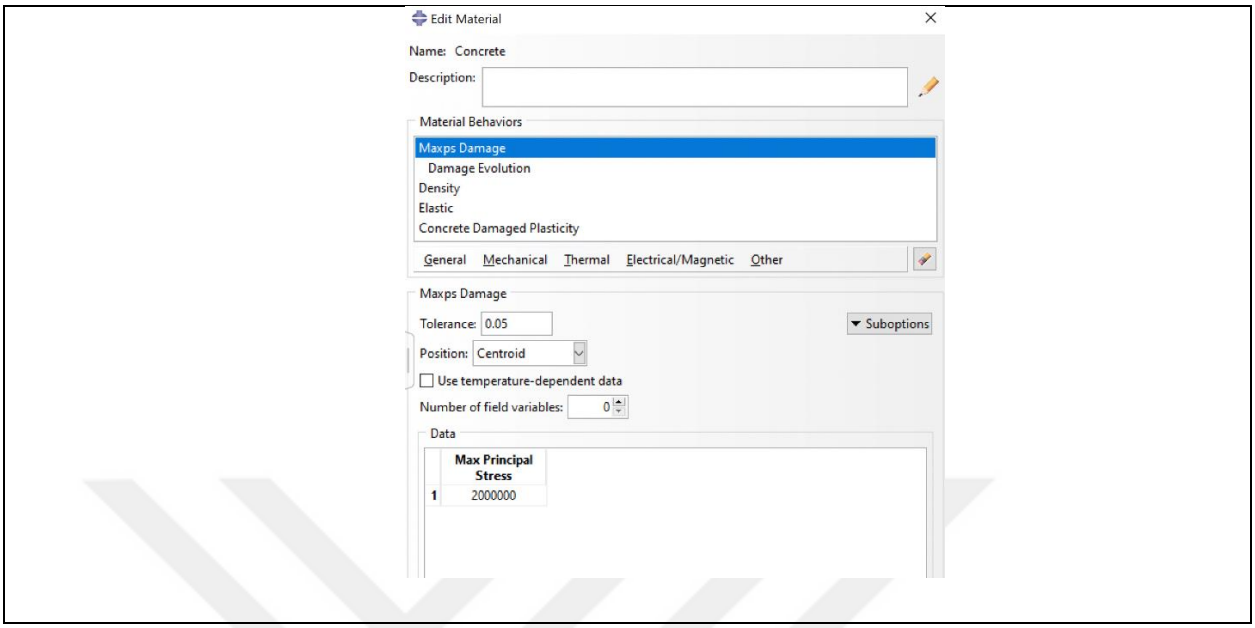

Figure 3.8: Concrete Material Properties used in the Simulation

Furthermore, specifications of damage evolution for crack propagation were shown in Fig. 3.9, where the displacement to failure value was set as 0.0001 to present that the crack will be propagated after the displacement reach to the aforementioned value. Also, the softening mechanism was identified as linear for the crack propagation in this simulation.

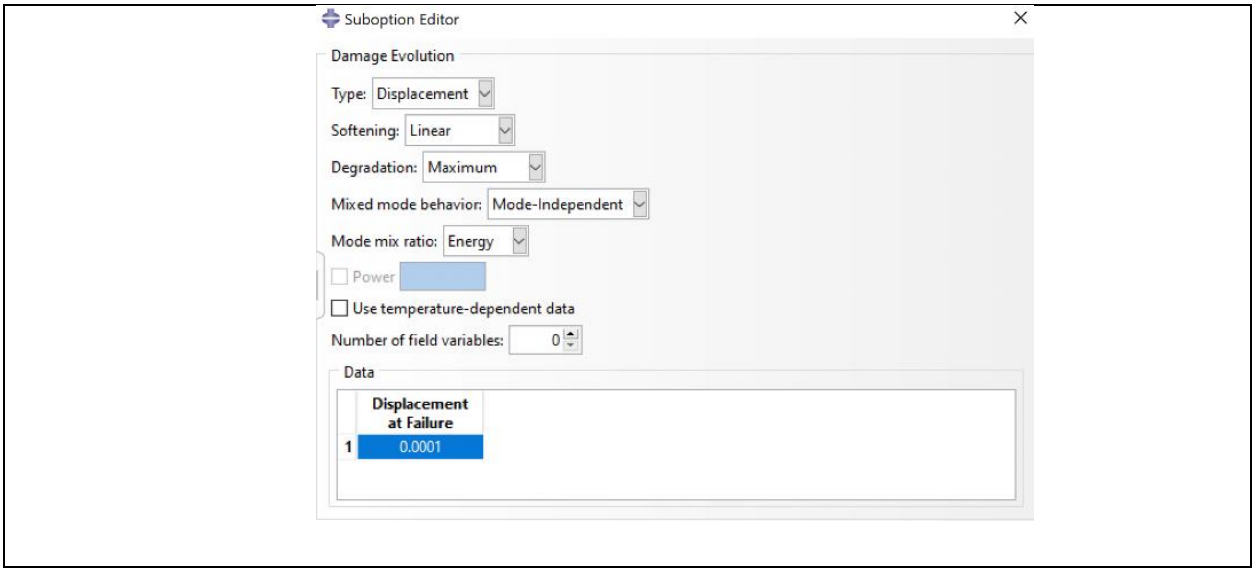

Figure 3.9: Specifications of Damage Evolution for Crack Propagation.

Finally, for the concrete material of the system, concrete damaged plasticity was defined based on the previous experimental studies. As it can be seen in Fig. 3.10, the stress and inelastic strain values at each stages of the experiment on the concrete have been tested and written in material properties module of ABAQUS (see Fig. 3.10).

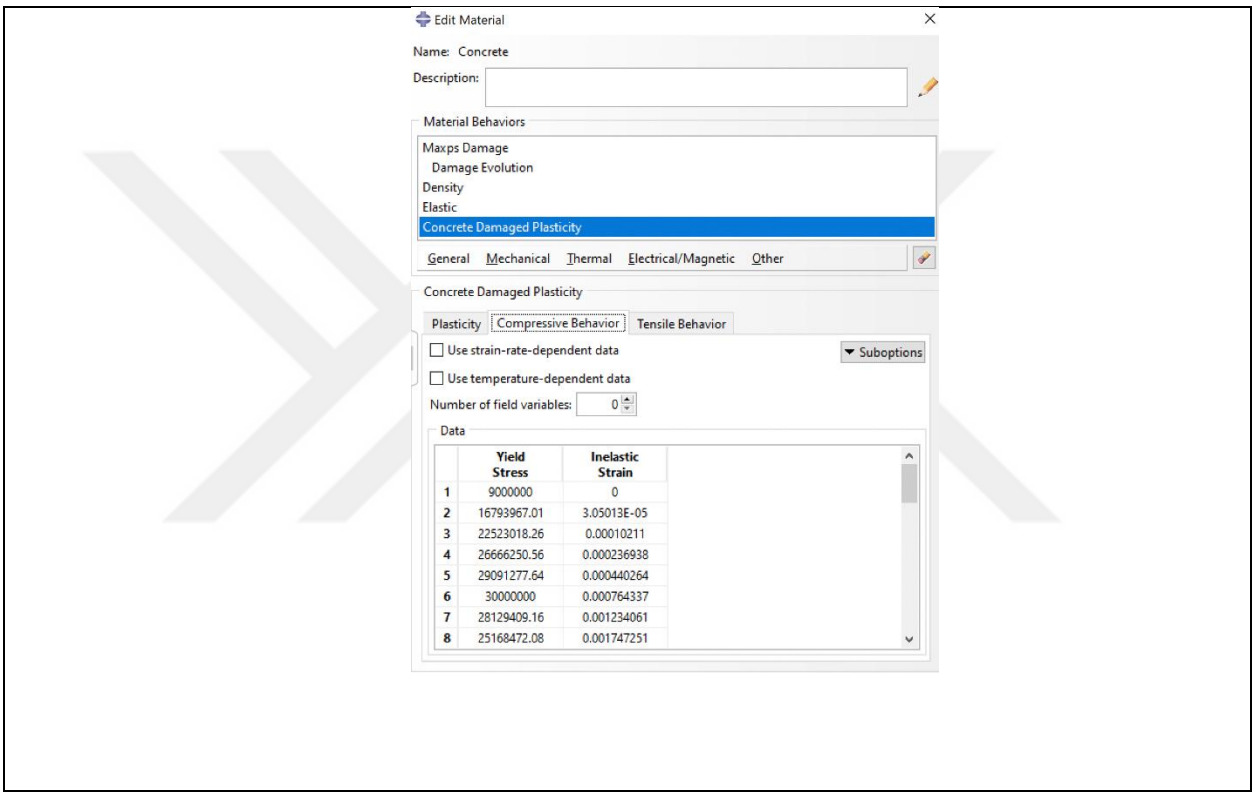

Figure 3.10: Concrete Damage Plasticity (CDP) Properties.

On the other hand, mechanical properties of fiber reinforced polymer used in this simulation as a reinforcement to cover the concrete have been defined in ABAQUS property module. As it is shown in Fig. 3.11, the density, elastic, and damage criteria such as Hashin damage were defined to specified the properties of the FRP.

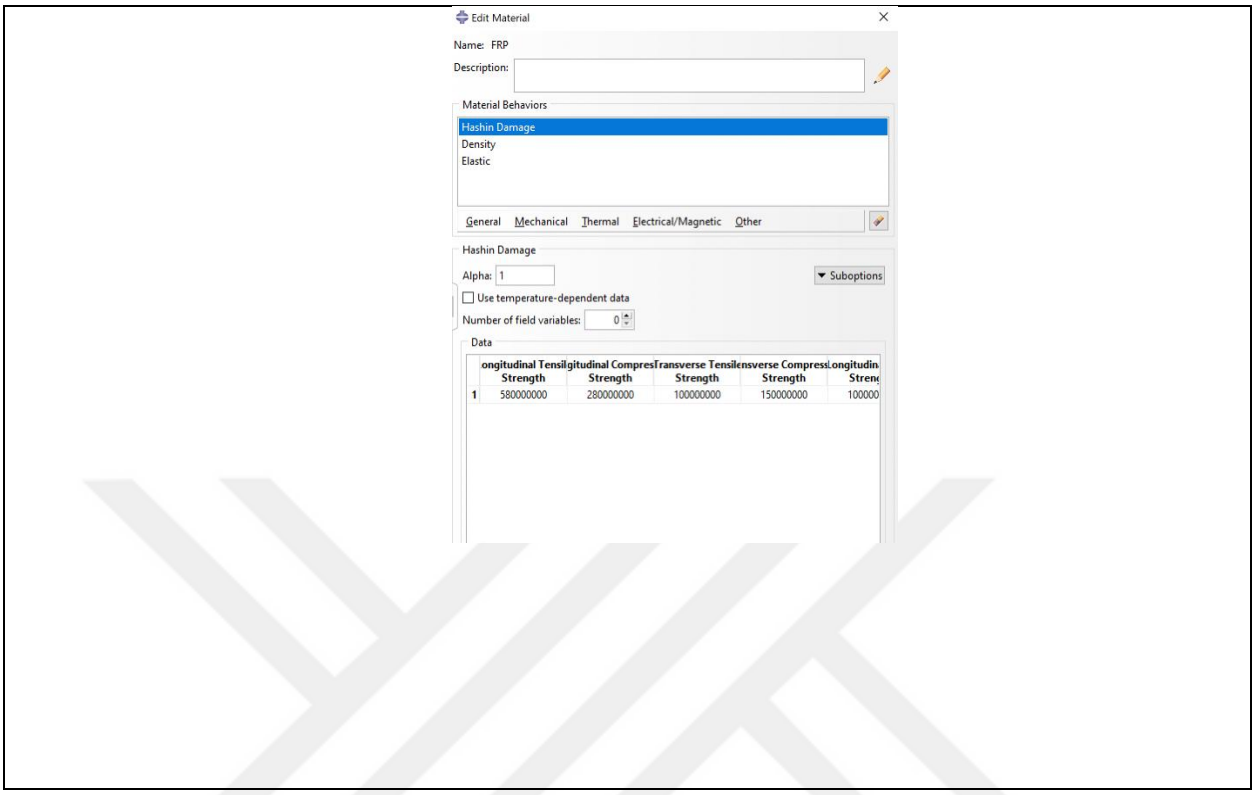

Figure 3.11: Mechanical Properties of CFRP as a Reinforcement to cover the concrete and damage criteria such as HASHIN damage

Also, the profile diameters of the bars and stirrups for the steel reinforcement in embedded section were chosen based on the design of the reinforcement concrete beams in the experimental studies (see Fig. 3.12).

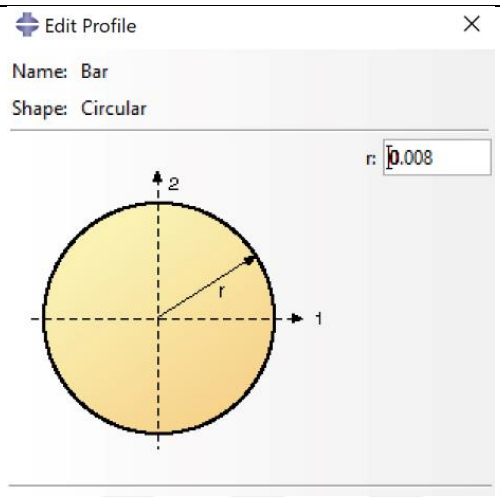

Figure 3.12: Defining the Profile Diameters of the bars and stirrups for the steel reinforcement embedded part.

3.1.4 Step and Interaction Module

In this section the interactions between all the parts of the setup were defined and friction properties also was added between the concrete and CFRP reinforcement material. Also, between supports and beam the encastre boundary conditions were defined, so the beam can just deform and slip on the support, therefore, support will be fixed.

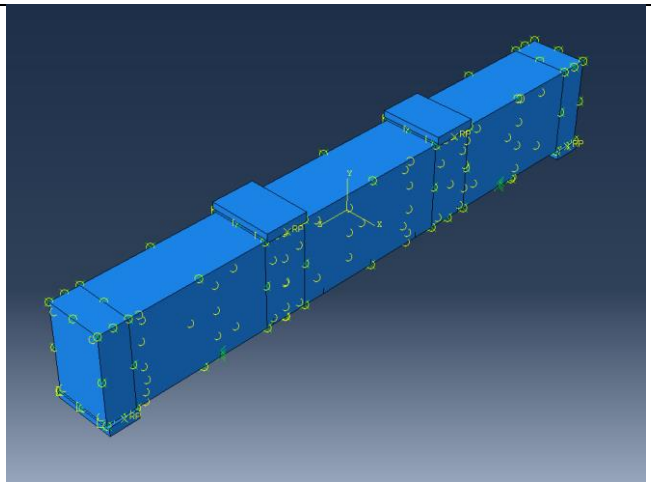

Figure 3.13: The Interactions Defined to the System between all the parts

3.1.5 Load Module

In the load module of the software, as it shown in Fig. 3.14, the location of the loads applied on the beam and also the encastre support were set as illustrated. This setup usually works using a hydraulic jack in order to apply the load from two parts on the center of the beam.

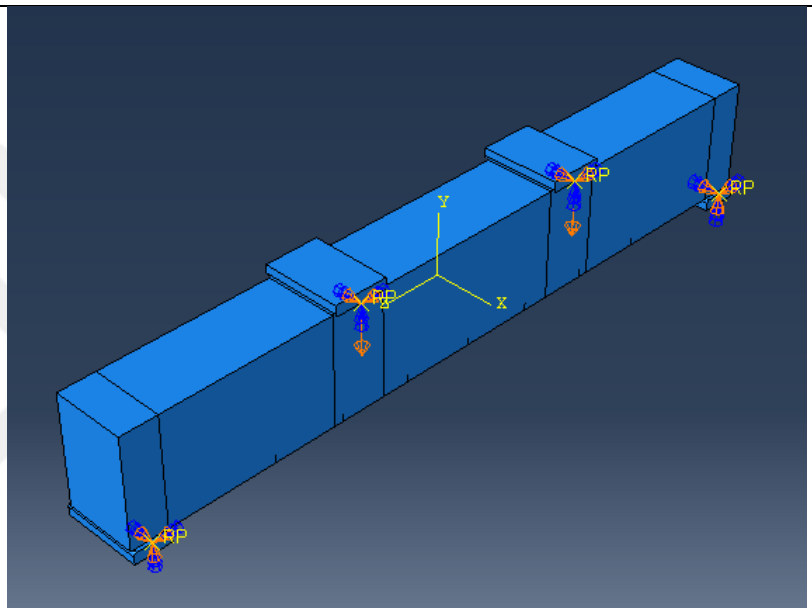

Figure 3.14: The Location of the Applied Loads and Supports of the Beam.

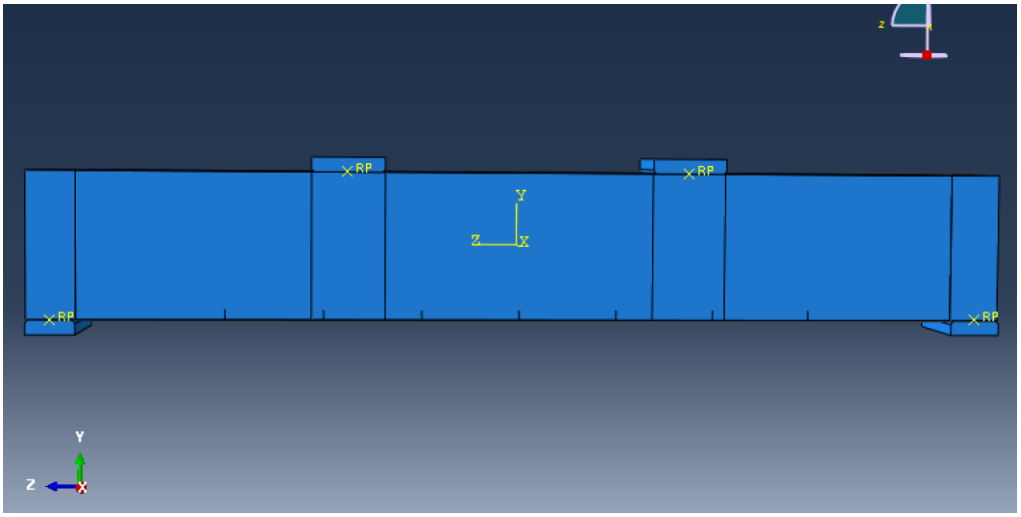

Figure 3.15: Side View of the RCB with Cracks on the Bottom Part of the Beam.

4. RESULTS AND DISCUSSION

As mentioned in the previous chapter, the CFRP laminated reinforcements were used in the simulation in order to repair and decrease the crack initiation and subsequently crack propagation in the tension part of the concrete beams. In order to find the most optimum parameters for the FRP reinforcement, different optimization systems were employed. To do this, Taguchi's optimization method was used to optimize the dimension of the FRP reinforcement covered bottom part of the beam. L9 orthogonal array was chosen from the various types of Taguchi method in order to minimize the number of simulations. The parameters with the levels for each of them have been listed in Table 4.1. Three parameters of width, length, and thickness of FRP were used as the variables, and three levels for each of these parameters were selected to fill the simulation sets.

Table 4.1: Dimensions of the FRP Layer to Repair the Bottom part of the RCB.

Parameter	Level 1 (mm)	Level 2 (mm)	Level 3 (mm)
Length	1400	1800	2000
Width	100	150	200
Thickness	0.5	1	2

After applying L9 orthogonal array Taguchi method, the experimental set of parameters were selected as shown in Table 4.2.

Minitab V20.4 was used to create the Taguchi analysis design with aforementioned parameters and level sets. Also, the maximum load at failure was selected as the response factor of the simulation sets.

Table 4.2: Simulation Set Numbers with Respective Parameters.

Simulation Set Number	Length (mm)	Width (mm)	Thickness (mm)
1	1400	100	0.5
2	1400	150	1.0
3	1400	200	2.0
4	1800	100	1.0
5	1800	150	2.0
6	1800	200	0.5
7	2000	100	2.0
8	2000	150	0.5
9	2000	200	1.0

All the conditions were simulated using the same initial crack patterns and the load at failure of the beam was exported from the ABAQUS software results, and subsequently the load vs deflection curves were formed in Origin Pro 2021b software. The results of the simulations for each condition are as follows:

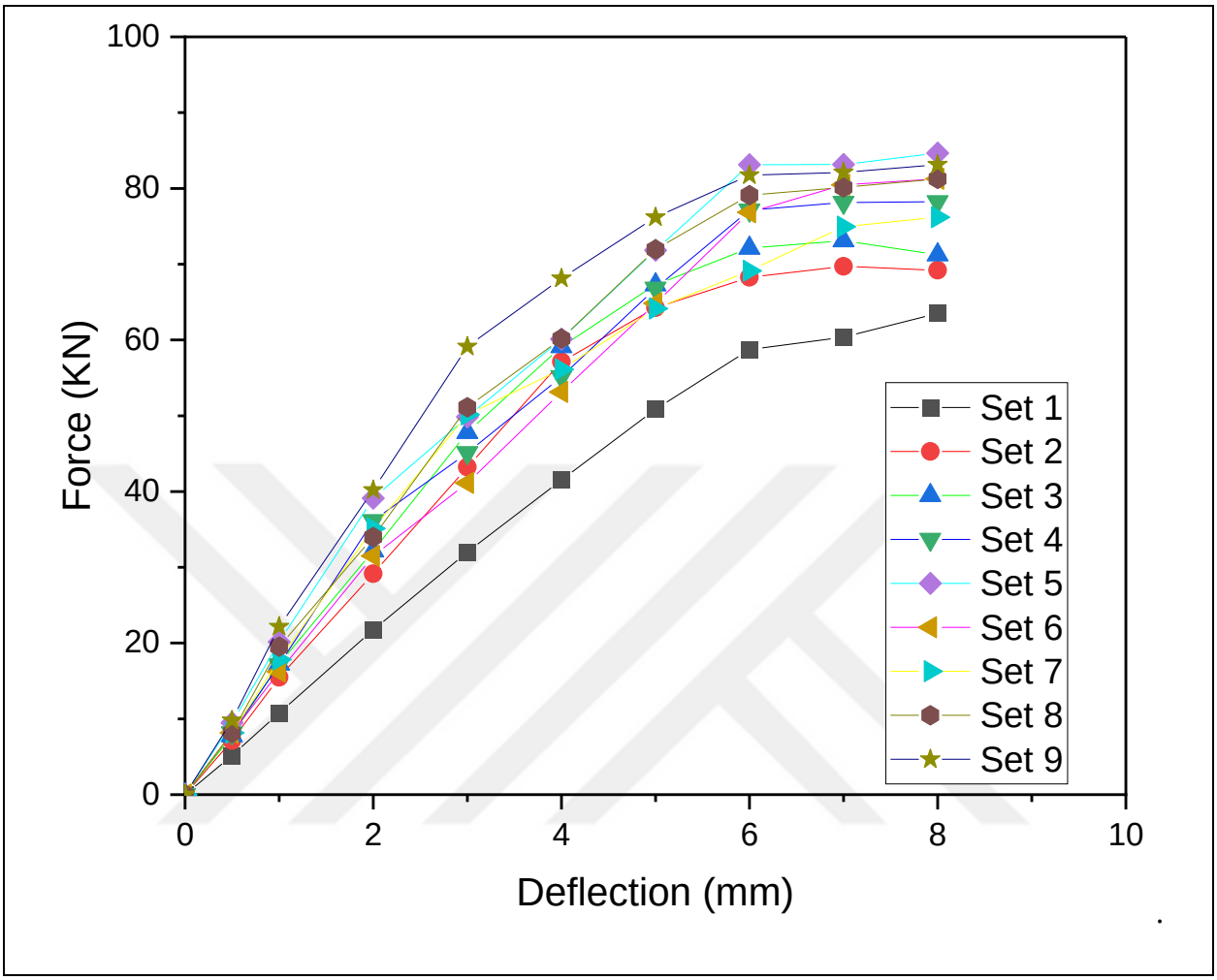

Figure 4.1: Force vs Deflection Curves of different simulation sets

It can be seen the highest force at the failure value is related to the set 5 parameters with length, width, and thickness of 1800, 150, and 2 mm, respectively. This can be attributed to the effect of covering all the length of the beam at the bottom surface of the beam as well as the high effect of 2 mm thickness on the increasing the strength of the pre-cracked RCB against the tension applied on the downside of the beam in flexural loading. Also, it can be asserted that increasing the width of the CFRP layer is not necessary after 150mm due to the blocking effect of the layer on the cracks throughout the length of the beam which can cover all the cracks. Also, based on the results of the flexural loading simulation, it can be concluded that covering all the beam length through the supports at both sides are not necessary and even can decrease the effect of the CFRP layer. This can be due to the softening effect of the polymer layer in the interaction points between the supports and beam where this layer can be torn in the edge of the supports.

The response factor was set as force at the failure in L9 orthogonal array Taguchi method and based on the results of the simulations, the response table for means was exported and shown in Table 4.3. Furthermore, the main effect plot for means was extracted from Minitab and demonstrated in Fig. 4.2. As it shown in the curves, it can be seen that the effect of increasing length of the CFRP layer from 1400mm to 1800mm was very critical to increase the force at the failure value. However, after reaching to the support part there is no need to increase the length up to the end of the beam.

Table 4.3: Response Table for Means Extracted from Minitab software for L9 orthogonal array Taguchi method.

Response Table for Means

Level	Length	Width	Thickness
1	67.99	72.65	75.35
2	81.38	78.38	76.86
3	80.20	78.55	77.36
Delta	13.39	5.90	2.02
Rank	1	2	3

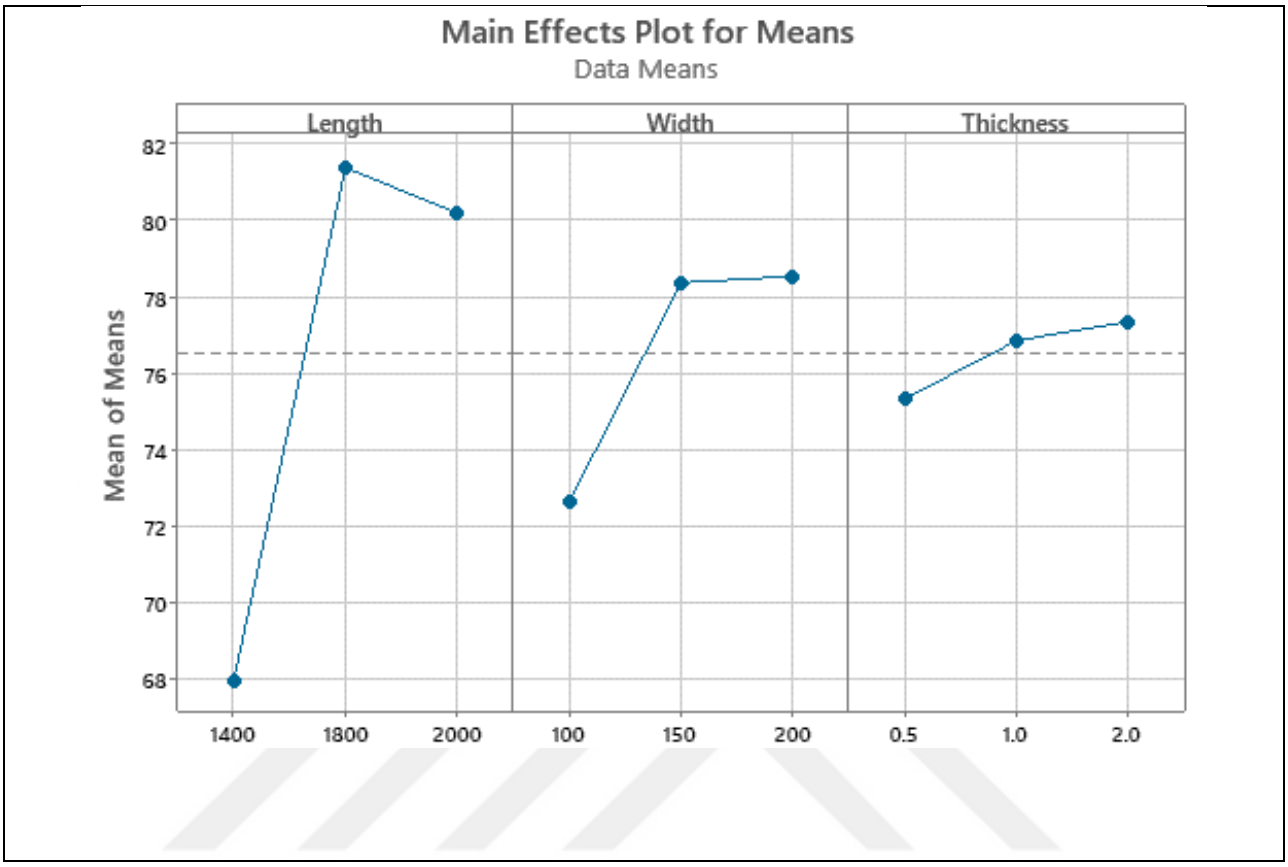

Figure 4.2: Main Effects plot for Means in L9 Orthogonal array Taguchi method exported from Minitab software

Moreover, it can be observed from the main effect plot for means that there is a sharp increase in force to failure when the width and thickness increase from 100 mm and 0.5 mm to 150 mm and 1 mm, respectively. However, the slope of the curve reduced after the aforementioned level, which means that there is no need to increase the size of the CFRP layer after this level because the rate of change may be not economical after this level. This can be attributed to the covering the main cracks along the beam with 150mm width. Also, the outside layer of the CFRP cannot affect too much on propagation of the pre-defined cracks, therefore, increasing the thickness from 1 to 2 mm is not necessary.

Fig. 4.3 illustrates the yielding of the reinforced concrete beam without any repair with other FRP materials. As it can be seen in Fig. 4.3, the cracks have been started from both side of the beam were the loads are applying from there but in the tension part due to low resistance to tensile force of the concrete. Subsequently, the cracks were diagonally propagated to the load implemented zones on the top of the beam. The outcomes of the simulation of the beam were in a decent agreement with the previous experimental and analytical studies in the aspect of starting the yield and propagation direction. Furthermore, with increasing deflection the cracks reach to the compressive parts and mixed with the cracks initiated from the compressive stress, and the failure happen.

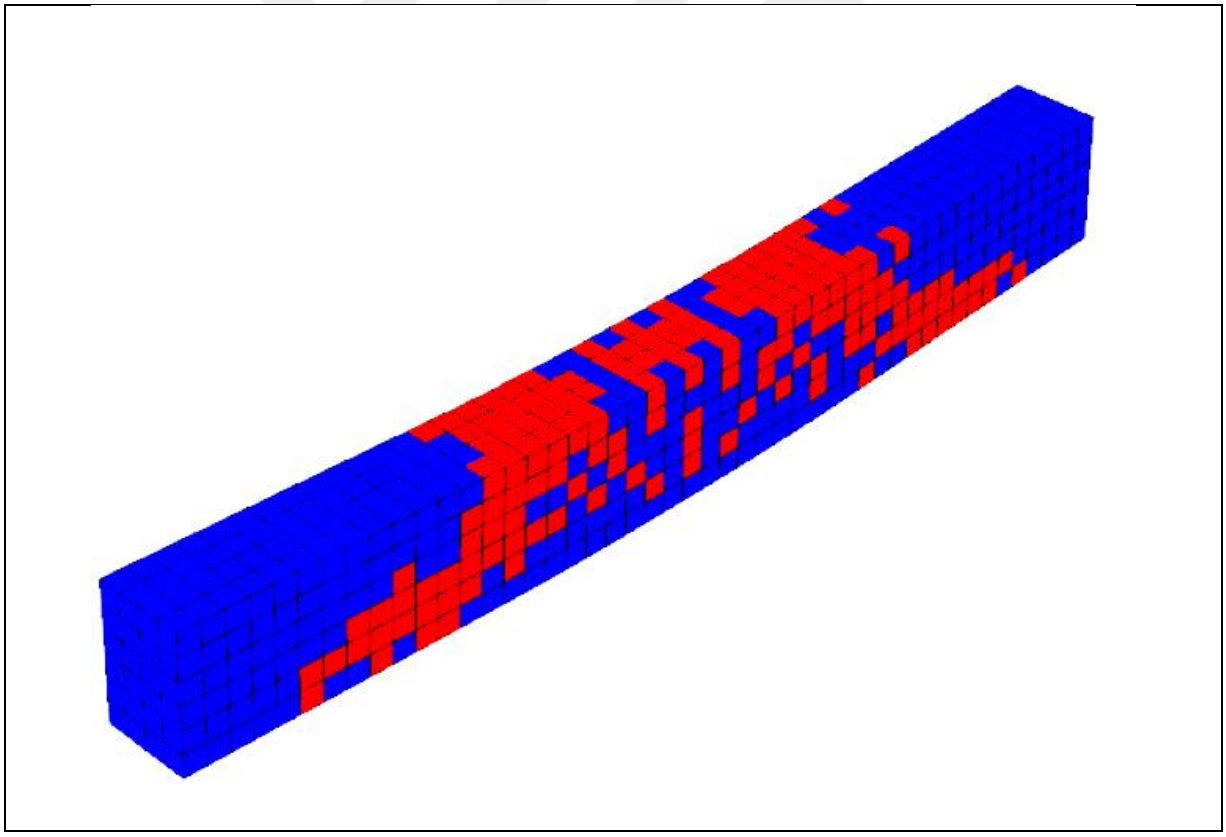

Figure 4.3: Yielding and Crack Propagation of RCB

Fig. 4.4 illustrates the yielding and crack propagation behavior of the NSM-CFRP reinforced RCB. It can be observed that the same crack propagation rout has been formed on the beam with a tendency to concentrate on the outside of the beam more than inside cracks.

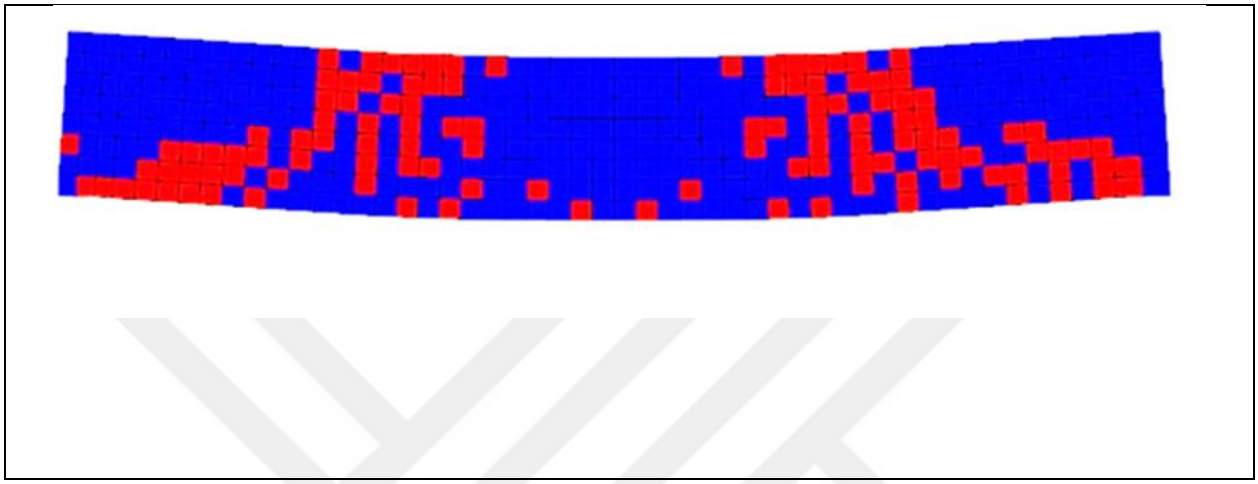

Figure 4.4: Yielding and crack propagation of NSM-CFRP reinforced RCB with laminated layer of 1800*150*1mm dimensions

5. CONCLUSIONS

In this paper the effect of CFRP dimensions on the flexural behavior of the reinforced concrete beam were investigated using numerical analysis. To this end, L9 orthogonal array Taguchi method was used to set the parameters of each condition. Minitab V20.4 was used to create the Taguchi analysis design with aforementioned parameters and level sets. The response factor was chosen as force to failure after 8 mm deflection and the main conclusions were as follows:

a) The highest force at the failure value is related to the set 5 parameters with length, width, and thickness of 1800, 150, and 2 mm, respectively which can be due to the effect of covering all the length of the beam at the bottom surface of the beam as well as the high effect of 2 mm thickness on the increasing the strength of the pre-cracked RCB against the tension applied on the downside of the beam in flexural loading.
b) Also, it can be asserted that increasing the width of the CFRP layer is not necessary after 150mm due to the blocking effect of the layer on the cracks throughout the length of the beam which can cover all the cracks.
c) Furthermore, based on the results of the flexural loading simulation, it can be concluded that covering all the beam length through the supports at both sides are not necessary and even can decrease the effect of the CFRP layer.
d) Moreover, the effect of increasing the width and thickness of the layer became steady after reaching to the middle level of 150 and 2 mm, respectively. This can be attributed to the covering the main cracks along the beam with 150mm width.

REFERENCES

[1] C. W. J. A. C. CONCRETING, "ACI 306R-16," 2017.

[2] E. G. Nawy, *Reinforced concrete*. Prentice-Hall, 1985.

[3] B. Bresler and A. C. Scordelis, "Shear strength of reinforced concrete beams," in *Journal Proceedings*, 1963, vol. 60, no. 1, pp. 51-74.

[4] D. Ngo and A. C. Scordelis, "Finite element analysis of reinforced concrete beams," in *Journal Proceedings*, 1967, vol. 64, no. 3, pp. 152-163.

[5] A. Placas, "Shear failure of reinforced concrete beams," 1971.

[6] T. Shioya, M. Iguro, Y. Nojiri, H. Akiyama, and T. J. S. P. Okada, "Shear strength of large reinforced concrete beams," vol. 118, pp. 259-280, 1990.

[7] P. H. J. J. o. C. f. C. Bischoff, "Deflection calculation of FRP reinforced concrete beams based on modifications to the existing Branson equation," vol. 11, no. 1, pp. 4-14, 2007.

[8] O. Buyukozturk and B. J. J. o. c. f. c. Hearing, "Failure behavior of precracked concrete beams retrofitted with FRP," vol. 2, no. 3, pp. 138-144, 1998.

[9] M. El-Mogy, A. El-Ragaby, and E. J. J. o. C. f. C. El-Salakawy, "Flexural behavior of continuous FRP-reinforced concrete beams," vol. 14, no. 6, pp. 669-680, 2010.

[10] I. F. Kara and A. F. J. C. s. Ashour, "Flexural performance of FRP reinforced concrete beams," vol. 94, no. 5, pp. 1616-1625, 2012.

[11] D. J. Oehlers, M. Mohamed Ali, M. Haskett, W. Lucas, R. Muhamad, and P. J. J. o. C. f. C. Visintin, "FRP-reinforced concrete beams: unified approach based on IC theory," vol. 15, no. 3, pp. 293-303, 2011.

[12] W. M. J. J. o. S. E. Sebastian, "Significance of midspan debonding failure in FRP-plated concrete beams," vol. 127, no. 7, pp. 792-798, 2001.

[13] A. K. Tureyen and R. J. J. S. J. Frosch, "Shear tests of FRP-reinforced concrete beams without stirrups," vol. 99, no. 4, pp. 427-434, 2002.

[14] F. Abed and A. R. J. C. S. Alhafiz, "Effect of basalt fibers on the flexural behavior of concrete beams reinforced with BFRP bars," vol. 215, pp. 23-34, 2019.

[15] S. H. J. C. Alsayed and C. Composites, "Flexural behaviour of concrete beams reinforced with GFRP bars," vol. 20, no. 1, pp. 1-11, 1998.

[16] A. J. C. Ashour and B. Materials, "Flexural and shear capacities of concrete beams reinforced with GFRP bars," vol. 20, no. 10, pp. 1005-1015, 2006.

[17] E. Atutis, J. Valivonis, and M. J. C. S. Atutis, "Deflection determination method for BFRP prestressed concrete beams under fatigue loading," vol. 226, p. 111182, 2019.

[18] R. Barnes and J. J. J. o. c. f. c. Fidell, "Performance in fire of small-scale CFRP strengthened concrete beams," vol. 10, no. 6, pp. 503-508, 2006.

[19] Q. Cao, J. Zhou, Z. Wu, and Z. J. J. E. S. Ma, "Flexural behavior of prestressed CFRP reinforced concrete beams by two different tensioning methods," vol. 189, pp. 411-422, 2019.

[20] M. M. Rafi, A. Nadjai, F. Ali, D. J. C. Talamona, and B. Materials, "Aspects of behaviour of CFRP reinforced concrete beams in bending," vol. 22, no. 3, pp. 277-285, 2008.

[21] H. A. Toutanji and M. J. S. J. Saafi, "Flexural behavior of concrete beams reinforced with glass fiber-reinforced polymer (GFRP) bars," vol. 97, no. 5, pp. 712-719, 2000.

[22] L. Zhou, Y. Zheng, G. Song, D. Chen, Y. J. C. Ye, and B. Materials, "Identification of the structural damage mechanism of BFRP bars reinforced concrete beams using smart transducers based on time reversal method," vol. 220, pp. 615-627, 2019.

[23] D. L. Logan, *A first course in the finite element method*. Cengage Learning, 2016.

[24] O. Chaallal, M.-J. Nollet, and D. J. C. J. o. C. E. Perraton, "Strengthening of reinforced concrete beams with externally bonded fiber-reinforced-plastic plates: design guidelines for shear and flexure," vol. 25, no. 4, pp. 692-704, 1998.

[25] T. C. J. A. s. j. Triantafillou, "Shear strengthening of reinforced concrete beams using epoxy-bonded FRP composites," vol. 95, pp. 107-115, 1998.

[26] Z. Zhang, C.-T. T. Hsu, and J. J. J. o. C. f. C. Moren, "Shear strengthening of reinforced concrete deep beams using carbon fiber reinforced polymer laminates," vol. 8, no. 5, pp. 403-414, 2004.

[27] S. Mau and T. S. T. J. S. J. Hsu, "Formula for the shear strength of deep beams," vol. 86, no. 5, pp. 516-523, 1989.

[28] M. Islam, M. Mansur, M. J. C. Maalej, and C. Composites, "Shear strengthening of RC deep beams using externally bonded FRP systems," vol. 27, no. 3, pp. 413-420, 2005.

[29] I. Ahmad, Z. Zhu, and A. J. J. o. C. f. C. Mirmiran, "Behavior of short and deep beams made of concrete-filled fiber-reinforced polymer tubes," vol. 12, no. 1, pp. 102-110, 2008.

[30] Z. Omeman, M. Nehdi, and H. J. C. J. o. C. E. El-Chabib, "Experimental study on shear behavior of carbon-fiber-reinforced polymer reinforced concrete short beams without web reinforcement," vol. 35, no. 1, pp. 1-10, 2008.

[31] S. Park and R. S. J. J. o. s. e. Aboutaha, "Strut-and-tie method for CFRP strengthened deep RC members," vol. 135, no. 6, pp. 632-643, 2009.

[32] J. G. MacGregor, J. K. Wight, S. Teng, and P. Irawan, *Reinforced concrete: Mechanics and design*. Prentice Hall Upper Saddle River, NJ, 1997.

[33] S. J. Foster and R. I. J. S. J. Gilbert, "The design of nonflexural members with normal and high-strength concretes," vol. 93, no. 1, pp. 3-10, 1996.

[34] F. J. Vecchio and M. P. J. J. o. s. e. Collins, "Compression response of cracked reinforced concrete," vol. 119, no. 12, pp. 3590-3610, 1993.

[35] T. El Maaddawy and S. J. C. S. Sherif, "FRP composites for shear strengthening of reinforced concrete deep beams with openings," vol. 89, no. 1, pp. 60-69, 2009.

[36] M. Andermatt, "Concrete deep beams reinforced with internal FRP," 2010.

[37] H.-K. Lee, S. Cheong, S.-K. Ha, and C. J. C. S. Lee, "Behavior and performance of RC T-section deep beams externally strengthened in shear with CFRP sheets," vol. 93, no. 2, pp. 911-922, 2011.

[38] U. s. M. ABAQUS and C. U. s. Manual, "Dassault Systemes Simulia Corp," *Providence, RI, USA*, vol. 6, no. 1, 2012.

[39] J. Lee and G. L. Fenves, "Plastic-Damage Model for Cyclic Loading of Concrete Structures," *Journal of Engineering Mechanics*, vol. 124, no. 8, pp. 892-900, 1998.

[40] S. Bahij, S. K. Adekunle, M. Al-Osta, S. Ahmad, S. U. Al-Dulaijan, and M. K. Rahman, "Numerical investigation of the shear behavior of reinforced ultra-high-performance concrete beams," *Structural Concrete*, vol. 19, no. 1, pp. 305-317, 2018.

[41] A. S. U. s. Manual, "Abaqus 6.11," *http://130.149*, vol. 89, no. 2080, p. v6, 2012.

[42] M. Barbato, "Efficient finite element modelling of reinforced concrete beams retrofitted with fibre reinforced polymers," *Computers & Structures*, vol. 87, no. 3-4, pp. 167-176, 2009.